Dynamical mean-field theory of spiking neuron ensembles: Response to a single spike with independent noises

Hideo Hasegawa*
Department of Physics, Tokyo Gakugei University, Koganei, Tokyo 184-8501, Japan
(Received 13 June 2002; revised manuscript received 26 December 2002; published 10 April 2003)

A semianalytical dynamical mean-field theory has been developed for a study of dynamics of an ensemble of N-unit FitzHugh-Nagumo neurons subject to white noises. Assuming weak noises and the Gaussian distribution of state variables, we have driven equations of motions for moments of *local* and *global* variables. Dynamical mean-field approximation (DMA) has replaced original, $2N$-dimensional stochastic differential equations (DEs) by eight-dimensional deterministic DEs, whereas the conventional moment method yields $N(2N+3)$-dimensional deterministic DEs for local variables. We have discussed the dependence of the spike firing precision and the synchronization on the noise intensity, synaptic coupling, and the size of the neuron ensemble. The spike timing precision is shown to be improved by increasing the size of the neuron ensemble, even when there are no couplings among neurons. When the coupling is introduced, neurons in ensembles respond to an input spike with a partial synchronization. Results calculated by our DMA theory are in good agreement with those obtained by direct simulations. DMA theory is extended to a large cluster which can be divided into multiple subclusters according to their functions. A model calculation has demonstrated that when the noise intensity is moderate, the spike propagation with a fairly precise timing is possible among noisy subclusters with feed-forward couplings, as in the synfire chain. We have compared DMA theory with the conventional moment method, showing that the former may be alternatively derived from the latter by a reduction in the number of moments with the mean-field approximation.

DOI: 10.1103/PhysRevE.67.041903 PACS number(s): 87.10.+e, 84.35.+i, 05.45.−a, 07.05.Mh

I. INTRODUCTION

It has been controversial that how neurons communicate information by firings or spikes [1–6]. Many debates on the nature of the neural code have been focused mainly on the two issues. The first issue is whether information is encoded in the average firing rate of neurons (*rate code*) or in the precise firing times (*temporal code*). Adrian [7] first noted the relationship between the neural firing rate and the stimulus intensity, which forms the basis of the rate code. Actually firing activities of motor and sensory neurons are reported to vary in response to applied stimuli. In recent years, however, an alternative temporal code has been proposed in which detailed spike timings are assumed to play an important role in information transmission: information is encoded in interspike intervals or in relative timings between firing times of spikes [8–10]. Indeed, experimental evidences have accumulated in the past several years, indicating a use of the temporal coding in neural systems [11–15]. Human visual systems, for example, have shown to classify patterns within 250 ms despite the fact that at least ten synaptic stages are involved from retina to the temporal brain [15]. The transmission times between two successive stages of synaptic transmission are suggested to be no more than 10 ms on the average. This period is too short to allow rates to be determined accurately.

The second issue is whether information is encoded in the activity of a single (or very few) neuron or that of a large number of neurons (*population* or *ensemble code*). The population rate-code model assumes that information is coded in the relative firing rates of ensemble neurons, and has been adopted in most of the theoretical analysis [16]. On the contrary, in the population temporal-code model, it is assumed that relative timings between spikes in ensemble neurons may be used as an encoding mechanism for perceptional processing [17–19]. A number of experimental data supporting this code have been reported in recent years [20,21]. For example, data has demonstrated that temporally coordinated spikes can systematically signal sensory object feature, even in the absence of changes in firing rate of the spikes [22].

It is well known that neurons in brains are subject to various kinds of noises, which can alter the response of neurons in various ways. Although firings of a single neocortical neuron in *vitro* are precise and reliable, those in *vivo* are quite unreliable [23]. This is due to noisy environment in *viro*, which makes the reliability of neuron firings worse. The strong criticism against the temporal code is that spikes are vulnerable to noise, while the rate code performs robustly in the presence of noise but with limited information capacity. It has been shown, however, that the response of neurons is improved by background noises against our conventional wisdom. The typical example is the stochastic resonance (SR), in which weak noises enhance the transmission of subthreshold signals (for review, see Refs. [24,25]). It has been shown that noise of appropriate magnitude linearlizes the response of neurons, which leads to SR and maximizes input-output correlation, transformation, and coherence (for review, see Ref. [26]). Recently, it has been demonstrated that noises can enhance the firing-time reliability of neurons stimulated by weak periodic and aperiodic inputs [27–29]. We may expect that a population of neuron ensembles plays

*Email address: hasegawa@u-gakugei.ac.jp

important roles in the response of neurons subject to noises. Actually, SR in Hodgkin-Huxley (HH) neuron ensembles has been first demonstrated for a single spike by Pei, Wilkens, and Moss [30]. Subsequently, this pooling effect has been supported for aperiodic [31,32] and periodic (analog) signals [33] and for spike-train inputs [34,35]. Quite recently, SR for a transient spike signal in large-scale HH neuron ensembles has been studied by using the wavelet analysis [34]. It may be possible that the firing-time precision is also improved by increasing the size of neuron ensembles.

A small patch of cortex may contain thousands of similar neurons, each connecting with hundreds or thousands of other neurons in that same patch or in other patches. The underlying dynamics of individual neurons includes a variety of voltage dependent ionic channels which can be described by Hodgkin-Huxley-type differential equations. Computational neuroscientists have so far tried to gain understanding of the properties of neuron ensembles with the use of two approaches: (i) direct simulations and (ii) analytical approaches such as mean-field (MF) theories and the Fokker-Plank equation (FPE). Simulations have been made for large-scale networks mostly consisting of integrate-and-fire (IF) neurons. Since the time to simulate networks by conventional methods grows as N^2 with N, the size of the network [36], it is rather difficult to simulate realistic neuron clusters, in spite of recent computer development. In MF theories [37–40], dynamics of globally coupled large-scale networks is described by a flow of phases or the population activity, which determines the fraction of the firing rate of neurons. The stability condition for synchronous and asynchronous states of neuron clusters has been investigated. Quite recently, the population density method has been developed as a modeling tool for large-scale neuronal clusters [41,42]. In these MF approaches, the macroscopic variable of interest is the firing rate following the *rate-code* hypothesis. However, only little MF approaches have so far been proposed based on the temporal-code hypothesis [39,40].

The purpose of the present study is to construct a dynamical mean-field approximation (DMA) theory based on the temporal-code hypothesis, generalizing the method previously proposed by Rodriguez and Tuckwell (RT) [43–46]. In the RT theory, the dynamics of the membrane potential of a neuron subject to white noises is studied by replacing *stochastic* differential equations (DEs) by *deterministic* DEs described by moments of state variables. RT's general theory has first been applied to a single FitzHugh-Nagumo (FN) neuron [43,44] and then a HH neuron [45,46]. In the case of a single FN neuron, two stochastic DEs are replaced by five deterministic DEs, for which an improvement to the RT theory has been recently proposed [47]. When the RT theory is applied to an N-unit FN neuron network, $2N$ stochastic DEs are replaced by $N_{eq}=N(2N+3)$ deterministic DEs [43,46]. In the case of $N=1000$, for example, we get $N_{eq}=2\,003\,000$, which is too large to perform calculations for realistic neuron ensembles. In their subsequent paper [45], the result of ensemble neurons is transplanted to FPE for the transition probability density, which is a partial DE with $2N+1$ independent variables. Solving such FPE is a hard computational task. We will present in this paper, an alternative MF theory for N-unit FN neuron ensembles, replacing $2N$ stochastic DEs by *eight* deterministic DEs which are expressed in terms of means, variances, and covariances of *local* and *global* state variables.

There are several nonlinear models which have been used for the study of neuron activities. Among them, we employ here the FN model [48,49] because it is relatively simple and amenable to analysis although the FN model does not have as firm an empirical basis as conductance-based model such as the HH model. The property of the FN model has been intensively investigated. In recent years, SR of a single FN neuron [50–52] and FN neuron ensembles [31,32,53,54] has been studied.

The paper is organized as follows. In Sec. II, we have developed a DMA theory for N-unit FN neuron ensembles, expanding stochastic DEs in terms of deviations from means in order to get equations of motions for variances and covariances of local and global variables. Comparing our DMA theory with the moment method [45], we show that the former may be alternatively derived from the latter by a reduction in the number of moments with the mean-field approximation. In Sec. III, some calculated results are reported of the response of ensemble neurons to a single spike with white noises. It will be shown that the spike firing precision is improved by increasing the ensemble size and the synaptic couplings, as expected. In Sec. IV, DMA theory is extended to a large cluster consisting of multiple subclusters and model calculations are reported. Finally, Sec. V is devoted to conclusions.

II. DYNAMICAL MEAN-FIELD APPROXIMATION

A. Basic formulation

We assume a neuron ensemble consisting of N-unit FN neurons. Dynamics of a single FN neuron i in a given ensemble is described by the nonlinear DEs given by

$$\frac{dx_i(t)}{dt}=F[x_i(t)]-cy_i(t)+\frac{w}{N}\sum_{j(\neq i)}G(x_j(t))+I^{(e)}(t)+\xi_i(t), \tag{1}$$

$$\frac{dy_i(t)}{dt}=bx_i(t)-dy_i(t)+e \quad (i=1-N), \tag{2}$$

where $F[x(t)]=k\,x(t)[x(t)-a][1-x(t)]$, $k=0.5$, $a=0.1$, $b=0.015$, $c=1.0$, $d=0.003$, and $e=0$ [43,44], and x_i and y_i denote the fast (voltage) and slow (recovery) variables, respectively. The third term in Eq. (1) stands for the couplings among neurons with the coupling strength w and the sigmoid function $G(x)=1/(1+\exp[-(x-\theta)/\alpha])$ with the threshold θ and the width α; the self-coupling terms are excluded and the normalization factor of N^{-1} is adopted instead of $(N-1)^{-1}$ for a later study of the $N=1$ limit. The fourth term of Eq. (1), $I^{(e)}(t)$, expresses an external, single spike input applied to all neurons, given by

$$I^{(e)}(t)=A\,\Theta(t-t_{in})\Theta(t_{in}+T_w-t), \tag{3}$$

where $\Theta(x)=1$ for $x>0$ and 0 otherwise, A stands for the magnitude, t_{in} the input time and T_w the spike width. The last term of Eq. (1), $\xi_i(t)$, denotes the independent Gaussian white noise with $\langle \xi_i(t)\rangle=0$ and $\langle \xi_i(t)\xi_j(t')\rangle=\beta^2\delta_{ij}\delta(t-t')$, the bracket $\langle\cdots\rangle$ denoting the average over stochastic random variables [see Eq. (8)].

After RT [43,44], we will express these nonlinear DEs by moments of variables. We define the global variables for the ensemble by

$$X(t)=\frac{1}{N}\sum_i x_i(t), \tag{4}$$

$$Y(t)=\frac{1}{N}\sum_i y_i(t), \tag{5}$$

and their averages by

$$\mu_1(t)=\langle X(t)\rangle, \tag{6}$$

$$\mu_2(t)=\langle Y(t)\rangle. \tag{7}$$

Here, the bracket of $\langle Q(\mathbf{z},t)\rangle$ denotes the average (or the expectation value) of an arbitrary function $Q(\mathbf{z},t)$ of N FN neuron ensembles defined by

$$\langle Q(\mathbf{z},t)\rangle=\int\cdots\int d\mathbf{z}Q(\mathbf{z},t)p(\mathbf{z}), \tag{8}$$

where $p(\mathbf{z})$ denotes a probability distribution function (pdf) for $2N$-dimensional random variables of $\mathbf{z}=(x_1,\ldots,x_N,y_1,\ldots,y_N)^t$. Rodriguez and Tuckwell [43] have shown that when $p(\mathbf{z})$ is given by the Gauss distribution concentrated near the mean point $\boldsymbol{\mu}$, we may expand $\langle Q(\mathbf{z},t)\rangle$ around $Q(\boldsymbol{\mu},t)$ in terms of the first and second moments of the variables. We express DEs given by Eqs. (1) and (2) in terms of the deviations from their averages defined by

$$\delta x_i(t)=x_i(t)-\mu_1(t), \tag{9}$$

$$\delta y_i(t)=y_i(t)-\mu_2(t), \tag{10}$$

to get (the argument t is hereafter suppressed)

$$\frac{dx_i}{dt}=F(\mu_1)+F'(\mu_1)\delta x_i+\tfrac{1}{2}F^{(2)}(\mu_1)\delta x_i^2+\tfrac{1}{6}F^{(3)}(\mu_1)\delta x_i^3 - c\mu_2-c\delta y_i+I_i^{(c)}+I_i^{(e)}+\xi_i, \tag{11}$$

$$\frac{dy_i}{dt}=b\mu_1-d\mu_2+b\delta x_i-d\delta y_i+e, \tag{12}$$

with

$$I_i^{(c)}=w\left(1-\frac{1}{N}\right)G(\mu_1)+\frac{w}{N}\sum_{j(\neq i)}\left[G'(\mu_1)\delta x_j+\frac{1}{2}G^{(2)}(\mu_1)\delta x_j^2+\frac{1}{6}G^{(3)}(\mu_1)\delta x_j^3\right]. \tag{13}$$

We define the variances and covariances between local variables given by

$$\gamma_{1,1}=\frac{1}{N}\sum_i\langle\delta x_i^2\rangle, \tag{14}$$

$$\gamma_{2,2}=\frac{1}{N}\sum_i\langle\delta y_i^2\rangle, \tag{15}$$

$$\gamma_{1,2}=\frac{1}{N}\sum_i\langle\delta x_i\delta y_i\rangle, \tag{16}$$

and those between global variables given by

$$\rho_{1,1}=\langle\delta X^2\rangle, \tag{17}$$

$$\rho_{2,2}=\langle\delta Y^2\rangle, \tag{18}$$

$$\rho_{1,2}=\langle\delta X\,\delta Y\rangle, \tag{19}$$

where $\delta X=X(t)-\mu_1(t)$ and $\delta Y=Y(t)-\mu_2(t)$. It is noted that $\gamma_{\kappa,\lambda}$ expresses the spatial average of fluctuations in local variables of x_i and y_i, while $\rho_{\kappa,\lambda}$ denotes fluctuations in global variables of X and Y ($\kappa,\lambda=1,2$).

We assume that the noise intensity β is weak and the distribution of state variables takes the Gaussian form. The first assumption allows us to expand the quantities in a power series of fluctuation moments around means. As for the second assumption, numerical simulations have shown that for weak noises, the distribution of $x(t)$ of the membrane potential of a single FN neuron nearly obeys the Gaussian distribution, although for strong noises, the distribution of $x(t)$ deviates from the Gaussian taking a bimodal form (see Fig. 8 of Ref. [44] and Fig. 3 of Ref. [47]). Similar behavior of the membrane-potential distribution has been reported also in a HH neuron model [27,28]. Furthermore, we adopt a mean-field approximation in which quantities averaged at a given site are assumed to be the same as their global averages. This type of approximations has been widely adopted in mean-field theories such as the Weiss theory for magnetism [55] and the coherent-potential approximation for random alloys [56]. When we adopt the Gaussian decoupling approximation and the mean-field approximation, averages of fluctuations are expressed in terms of the first and second moments only [Eqs. (A6)–(A9)]. After some manipulations, we get equations of motions for μ_κ, $\gamma_{\kappa,\lambda}$, and $\rho_{\kappa,\lambda}$ ($\kappa,\lambda=1,2$) given by (for details, see Appendix A)

$$\frac{d\mu_1}{dt}=f_0+f_2\gamma_{1,1}-c\mu_2+w\left(1-\frac{1}{N}\right)U_0+I^{(e)}(t), \tag{20}$$

$$\frac{d\mu_2}{dt}=b\mu_1-d\mu_2+e, \tag{21}$$

$$\frac{d\gamma_{1,1}}{dt}=2[(f_1+3f_3\gamma_{1,1})\gamma_{1,1}-c\gamma_{1,2}]+2w\left(\rho_{1,1}-\frac{\gamma_{1,1}}{N}\right)U_1+\beta^2, \tag{22}$$

$$\frac{d\gamma_{2,2}}{dt}=2(b\gamma_{1,2}-d\gamma_{2,2}), \tag{23}$$

$$\frac{d\gamma_{1,2}}{dt}=b\gamma_{1,1}+(f_1+3f_3\gamma_{1,1}-d)\gamma_{1,2}-c\gamma_{2,2}+w\left(\rho_{1,2}-\frac{\gamma_{1,2}}{N}\right)U_1, \tag{24}$$

$$\frac{d\rho_{1,1}}{dt}=2[(f_1+3f_3\gamma_{1,1})\rho_{1,1}-c\rho_{1,2}]+2w\left(1-\frac{1}{N}\right)\rho_{1,1}U_1+\frac{\beta^2}{N}, \tag{25}$$

$$\frac{d\rho_{2,2}}{dt}=2(b\rho_{1,2}-d\rho_{2,2}), \tag{26}$$

$$\frac{d\rho_{1,2}}{dt}=b\rho_{1,1}+(f_1+3f_3\gamma_{1,1}-d)\rho_{1,2}-c\rho_{2,2}+w\left(1-\frac{1}{N}\right)\rho_{1,2}U_1, \tag{27}$$

with

$$U_0=g_o+g_2\gamma_{1,1}, \tag{28}$$

$$U_1=g_1+3g_3\gamma_{1,1}, \tag{29}$$

$$f_\ell=\left(\frac{1}{\ell!}\right)F^{(\ell)}(\mu_1), \tag{30}$$

$$g_\ell=\left(\frac{1}{\ell!}\right)G^{(\ell)}(\mu_1). \tag{31}$$

The original $2N$-dimensional *stochastic* DEs given by Eqs. (1) and (2) are transformed to eight-dimensional *deterministic* DEs given by Eqs. (20)–(27), which show much variety depending on model parameters such as the strength of white noise (β), couplings (w), and the size of cluster (N).

B. Derivation of DMA theory from the moment method

Although DMA theory has been derived in preceding Sec. II A, from a calculation of equations of motions for means, variances, and covariances of local and global variables, we will show that DMA theory may be derived also from the moment method initiated by Rodriguez and Tuckwell [43]. For an N-unit FN neuron ensemble, the moment method defines means of variables of x_i and y_i for the neuron i given by

$$m_1^i=\langle x_i\rangle, \tag{32}$$

$$m_2^i=\langle y_i\rangle \tag{33}$$

for a calculation of variances and covariances between *local* variables given by

$$C_{1,1}^{i,j}=\langle\Delta x_i\Delta x_j\rangle, \tag{34}$$

$$C_{2,2}^{i,j}=\langle\Delta y_i\Delta y_j\rangle, \tag{35}$$

$$C_{1,2}^{i,j}=\langle\Delta x_i\Delta y_j\rangle, \tag{36}$$

where $\Delta x_i=x_i-m_1^i$ and $\Delta y_i=y_i-m_2^i$: variances are given by setting $i=j$. Adopting the assumptions of weak noises and the Gaussian distribution for state variables, we get DEs for these moments given by (for details see Appendix A)

$$\frac{dm_1^i}{dt}=f_0^i+f_2^iC_{1,1}^{i,i}-cm_2^i+\frac{w}{N}\sum_{k(\neq i)}[g_o^k+g_2^kC_{1,1}^{k,k}]+I^{(e)}, \tag{37}$$

$$\frac{dm_2^i}{dt}=bm_1^i-dm_2^i+e, \tag{38}$$

$$\frac{dC_{1,1}^{i,j}}{dt}=(f_1^i+3f_3^iC_{1,1}^{i,i}+f_1^j+3f_3^jC_{1,1}^{j,j})C_{1,1}^{i,j}-c(C_{1,2}^{i,j}+C_{2,1}^{i,j})+\beta^2\delta_{ij}+\frac{w}{N}\left[\sum_{k(\neq i)}(g_1^k+3g_3^kC_{1,1}^{k,k})C_{1,1}^{k,j}+\sum_{k(\neq j)}(g_1^k+3g_3^kC_{1,1}^{k,k})C_{1,1}^{i,k}\right], \tag{39}$$

$$\frac{dC_{2,2}^{i,j}}{dt}=b(C_{1,2}^{i,j}+C_{2,1}^{i,j})-2dC_{2,2}^{i,j}, \tag{40}$$

$$\frac{dC_{1,2}^{i,j}}{dt}=bC_{1,1}^{i,j}+(f_1^i+3f_3^iC_{1,1}^{i,i}-d)C_{1,2}^{i,j}-cC_{2,2}^{i,j}+\frac{w}{N}\sum_{k(\neq i)}(g_1^k+3g_3^kC_{1,1}^{k,k})C_{1,2}^{k,j}\quad(i,j=1\text{–}N), \tag{41}$$

where

$$f_\ell^i=\left(\frac{1}{\ell!}\right)F^{(\ell)}(m_1^i), \tag{42}$$

$$g_\ell^i=\left(\frac{1}{\ell!}\right)G^{(\ell)}(m_1^i). \tag{43}$$

The original RT theory [43] includes up to the second-order moments. The expression given by Eqs. (37)–(41), however, takes into account up to the fourth-order moments with the use of the Gaussian decoupling approximation [47]: RT's result may be given by Eqs. (37)–(41), but by setting $f_3^i=g_3^k=0$.

Comparing Eqs. (4)–(7) and (14)–(19) with Eqs. (32)–(36), we define the quantities given by

$$\overline{\mu}_\kappa = \frac{1}{N}\sum_i m_\kappa^i, \tag{44}$$

$$\overline{\gamma}_{\kappa,\lambda} = \frac{1}{N}\sum_i C_{\kappa,\lambda}^{i,i} + d_{\kappa,\lambda}, \tag{45}$$

$$\overline{\rho}_{\kappa,\lambda} = \frac{1}{N^2}\sum_i \sum_i C_{\kappa,\lambda}^{i,j} \quad (\kappa,\lambda = 1,2), \tag{46}$$

with

$$d_{\kappa,\lambda} = \frac{1}{N}\sum_i \delta m_\kappa^i \delta m_\lambda^i, \tag{47}$$

$$\delta m_\kappa^i = m_\kappa^i - \mu_\kappa, \tag{48}$$

where we employ the identities: $\delta x_i = \Delta x_i + \delta m_1^i$ and $\delta y_i = \Delta y_i + \delta m_2^i$. By using Eqs. (37)–(41) and (44)–(46), we get DEs for $d\overline{\mu}_\kappa/dt$, $d\overline{\gamma}_{\kappa,\lambda}/dt$, and $d\overline{\rho}_{\kappa,\lambda}/dt$ from the moment method. It may be shown that DEs obtained from the second-order moment method, where $f_3 = g_3 = 0$ in Eqs. (37)–(41), exactly agree with corresponding DEs in DMA. This is because DEs within the second-order moment approximation are linear functions of the first- and second-order moments, details being presented in Appendix B [Eqs. (B1)–(B8)]. In contrast, when the fourth-order moment terms in these DEs are linearized with the use of the Gaussian and mean-field approximations as given by Eqs. (B14)–(B16), results obtained from the fourth-order moment method again agree with those of DMA.

It is worthwhile to show that DMA theory may be more easily derived from the moment method when the following conditions are satisfied:

$$m_\kappa^i = m_\kappa, \tag{49}$$

$$C_{\kappa,\lambda}^{i,j} = \delta_{ij} C_{\kappa,\lambda} + (1-\delta_{ij})\hat{C}_{\kappa,\lambda}, \tag{50}$$

where m_κ denotes the constant value of m_κ^i independent of i, and $C_{\kappa,\lambda}$ and $\hat{C}_{\kappa,\lambda}$ stand for the intrasite and intersite terms of $C_{\kappa,\lambda}^{i,j}$, respectively. The conditions given by Eqs. (49) and (50) will be satisfied in excitable neuron ensembles with uniform couplings, where the variables in all neurons are in the rest state without external inputs, and nearest-neighbor sites and far-neighbor sites of a given neuron are indistinguishable. Substituting Eqs. (49) and (50) in Eqs. (44)–(46), we get

$$\overline{\mu}_\kappa = m_\kappa, \tag{51}$$

$$\overline{\gamma}_{\kappa,\lambda} = C_{\kappa,\lambda}, \tag{52}$$

$$\overline{\rho}_{\kappa,\lambda} = \frac{1}{N} C_{\kappa,\lambda} + \left(1 - \frac{1}{N}\right)\hat{C}_{\kappa,\lambda}. \tag{53}$$

We may show that $\mu_\kappa = \overline{\mu}_\kappa$, $\gamma_{\kappa,\lambda} = \overline{\gamma}_{\kappa,\lambda}$, and $\rho_{\kappa,\lambda} = \overline{\rho}_{\kappa,\lambda}$, which hold even within the fourth-order moment approximation.

For a single FN neuron ($N=1$), the moment method and DMA yield the same result (see Appendix B). For a pair of FN neurons ($N=2$), numbers of coupled DE equations are $N_{eq}=14$ and 8 in the moment and DMA methods, respectively, where we employ the symmetry relations such as $C_{\kappa,\lambda}^{1,2} = C_{\lambda,\kappa}^{2,1}$. A more detailed comparison between DMA and moment methods for the case of $N=2$ is provided in Appendix B with some numerical calculations.

For a general N-unit FN neuron ensemble, the number of coupled DEs in the moment method [Eqs. (37)–(41)] is $N_{eq} = 2N + N(2N+1) = N(2N+3)$, which is 230, 20 300, and 2 003 000 for $N=10$, 100, and 1000, respectively, while $N_{eq}=8$ independent of N in our DMA theory [Eqs. (20)–(27)]. Thus, N_{eq} in the moment method has the exponential N dependence, which prevents us from performing calculations for realistic neuron ensembles.

C. Property of DMA theory

The DMA theory successfully reduces the number of DEs, by taking account of μ_κ, $\gamma_{\kappa,\lambda}$, and $\rho_{\kappa,\lambda}$ for *global* variables as well as *local* variables instead of m_κ^i and $C_{\kappa,\lambda}^{i,j}$ for local variables. The moment method imposes no constraints on the coupling strength [43–46]. This is expected to be the case also for DMA theory, although it may become worse for stronger couplings because of the additionally introduced mean-field approximation. One of the advantages of the moment method over the DMA is that the former may take into account the intersite cross correlation between the different neurons such as $C_{\kappa,\lambda}^{i,j}$ for $i \neq j$, while DMA calculates the averaged quantities. The DMA, however, has advantages of a tractable small number of DEs and clear semianalytical nature, from which some qualitative results may be deduced without numerical calculations, as will be shown shortly [e.g., Eq. (57)]. DMA is expected to be better applied to larger N ensembles, which is inherent in mean-field theories [55,56].

1. Single-site self-consistent approximation

It is possible to regard DMA theory as the *single-site self-consistent* theory. Let us assume a configuration in which a *single* neuron i is embedded in an effective medium whose effect is realized by a given neuron i as its effective external input through the coupling w. We replace quantities of m_κ^k, $C_{\kappa,\lambda}^{k,k}$, and $(1/N)\Sigma_{k(\neq\ell)} C_{\kappa,\lambda\ell,k}$ in coupling terms of Eqs. (37)–(41) by *effective* quantities of μ_κ, $\gamma_{\kappa,\lambda}$, and $\rho_{\kappa,\lambda} - (1/N)\gamma_{\kappa,\lambda}$, respectively. Then, in order to determine these quantities just introduced, we impose the self-consistent condition given by [see Eqs. (44)–(46)]

$$\mu_\kappa = m_\kappa^i, \tag{54}$$

$$\gamma_{\kappa,\lambda} = C_{\kappa,\lambda}^{i,i}, \tag{55}$$

$$\rho_{\kappa,\lambda}-\frac{1}{N}\gamma_{\kappa,\lambda}=\frac{1}{N}\sum_{j(\neq i)}C^{i,j}_{\kappa,\lambda}. \tag{56}$$

Note that Eqs. (54)–(56) are assumed to hold independent of i and that m^i_κ and $C^{i,j}_{\kappa,\lambda}$ on their righthand sides are functions of μ_κ, $\gamma_{\kappa,\lambda}$, and $\rho_{\kappa,\lambda}$. The condition given by Eqs. (54)–(56) yields DEs for μ_κ, $\gamma_{\kappa,\lambda}$, and $\rho_{\kappa,\lambda}$ which are again given by Eqs. (20)–(27). The self-consistent condition given by Eqs. (54)–(56), which assumes that the quantities averaged at a given site are the same as those of the effective medium, is common in mean-field theories [55,56].

2. Firing-time distribution

We should note that the noise contribution is β^2 in Eq. (22), while that is β^2/N in Eq. (25). It is easy to see that

$$\rho_{\kappa,\lambda}=\begin{cases}\dfrac{\gamma_{\kappa,\lambda}}{N} & \text{for } w/\beta^2\to 0 \quad (57a)\\ \gamma_{\kappa,\lambda} & \text{for } \beta^2/w\to 0. \quad (57b)\end{cases}$$

Equation (57a) agrees with the *central-limit theorem*. Thus, the ratio $\rho_{\kappa,\lambda}/\gamma_{\kappa,\lambda}$ changes as model parameters are changed. We will show that these changes in $\rho_{\kappa,\lambda}$ and $\gamma_{\kappa,\lambda}$ reflect on the firing-time distribution and the degree of synchronous firings in neurons ensembles.

The nth firing time of a given neuron i in the ensemble is defined as the time when $x_i(t)$ crosses the threshold θ from below:

$$t_{oin}=\{t|x_i(t)=\theta;\dot{x}_i>0;t\geqslant t_{oin-1}+\tau_r\}, \tag{58}$$

where τ_r denotes the refractory period introduced so as to avoid multiple firings in a short period arising from fluctuations in voltage variables around the threshold. We get the distribution for the membrane-potential variable x_i given by (for details, see Appendix C)

$$P(x_i)\simeq\left(\frac{1}{\sigma_\ell}\right)\phi\left(\frac{x_i-\mu_1}{\sigma_\ell}\right), \tag{59}$$

where $\phi(x)$ is the normal distribution function given by

$$\phi(x)=\frac{1}{\sqrt{2\pi}}\exp\left(-\frac{x^2}{2}\right), \tag{60}$$

with

$$\sigma_\ell=\sqrt{\gamma_{1,1}}. \tag{61}$$

This implies that the distribution of the voltage variable $x_i(t)$ is described by the Gaussian distribution with the mean of $\mu_1(t)$ and the variance of $\gamma_{1,1}(t)$. The probability given by Eq. (59) depends on the time because of the time dependence of $x_i(t)$ and $\sigma_\ell(t)$. The probability $W_{oi}(t)$ when $x_i(t)$ at t is above the threshold θ is given by [43]

$$W_{oi}(t)=1-\psi\left(\frac{\theta-\mu_1}{\sigma_\ell}\right), \tag{62}$$

where $\psi(y)$ is the error function given by integrating $\phi(x)$ from $-\infty$ to y. Then the probability averaged over the ensemble is given by

$$W_\ell(t)=\frac{1}{N}\sum_i W_{oi}(t)=1-\psi\left(\frac{\theta-\mu_1}{\sigma_\ell}\right). \tag{63}$$

The fraction of a given neuron i emitting output spikes at t is given by

$$Z_\ell(t)=\frac{d\,W_\ell(t)}{dt}\Theta(\dot{\mu}_1)=\phi\left(\frac{\theta-\mu_1}{\sigma_\ell}\right)\frac{d}{dt}\left(\frac{\mu_1}{\sigma_\ell}\right)\Theta(\dot{\mu}_1), \tag{64}$$

where $\dot{\mu}_1=d\mu_1/dt$. When we expand $\mu_1(t)$ in Eq. (64) around t^*_o, where $\mu_1(t^*_o)=\theta$, it becomes

$$Z_\ell(t)\sim\phi\left(\frac{t-t^*_o}{\delta t_{o\ell}}\right)\frac{d}{dt}\left(\frac{\mu_1}{\sigma_\ell}\right)\Theta(\dot{\mu}_1), \tag{65}$$

with

$$\delta t_{o\ell}=\frac{\sigma_\ell}{\dot{\mu}_1}, \tag{66}$$

where μ_1, $\dot{\mu}_1$, and σ_ℓ are evaluated at $t=t^*_o$. $Z_\ell(t)$ provides the distribution of firing times showing that most of the firing times of neurons are located in the range given as

$$t_{o\ell}\in[t^*_o-\delta t_{o\ell},\ t^*_o+\delta t_{o\ell}]. \tag{67}$$

In the limit of vanishing β, Eq. (65) reduces to

$$Z_\ell(t)=\delta(t-t^*_o). \tag{68}$$

Similarly, we get the distribution for the global variable X given by (for details, see Appendix D)

$$P(X)\simeq\left(\frac{1}{\sigma_g}\right)\phi\left(\frac{X-\mu_1}{\sigma_g}\right), \tag{69}$$

with

$$\sigma_g=\sqrt{\rho_{1,1}}. \tag{70}$$

This implies that the distribution of global voltage variable $X(t)$ is described by the Gaussian distribution with the mean of $\mu_1(t)$ and the variance of $\rho_{1,1}(t)$. If we define the mth firing time relevant to the global variable $X(t)$ as

$$t_{gm}=\{t|X(t)=\theta;\dot{X}(t)>0;t\geqslant t_{gm-1}+\tau_r\}, \tag{71}$$

the fraction of firing around $t=t^*_o$ is given by

$$Z_g(t)=\phi\left(\frac{t-t^*_o}{\delta t_{og}}\right)\frac{d}{dt}\left(\frac{\mu_1}{\sigma_g}\right)\Theta(\dot{\mu}_1), \tag{72}$$

with

$$\delta t_{og} = \frac{\sigma_g}{\mu_1}. \tag{73}$$

Then most of t_{og} is located in the range given by

$$t_{og} \in [t_o^* - \delta t_{og},\ t_o^* + \delta t_{og}]. \tag{74}$$

Since $\rho_{1,1}$ is generally smaller than $\gamma_{1,1}$, we get $\sigma_g \leqslant \sigma_\ell$ and $\delta t_{0g} \leqslant \delta t_{o\ell}$. In particular, in the case of no couplings, Eqs. (57), (61), (66), (70), and (73) lead to

$$\delta t_{og} = \frac{\delta t_{o\ell}}{\sqrt{N}} \quad \text{for} \quad w = 0. \tag{75}$$

3. Synchronous response

Now we consider the quantity given by

$$R(t) = \frac{1}{N^2} \sum_{ij} \langle [x_i(t) - x_j(t)]^2 \rangle = 2(\gamma_{1,1} - \rho_{1,1}). \tag{76}$$

When all neurons are in the completely synchronous state, we get $x_i(t) = X(t)$ for all i, and then $R(t) = 0$. On the contrary, in the asynchronous (random) state, we get $R(t) = 2(1 - 1/N)\gamma_{1,1} \equiv R_0(t)$. Then the quantity defined by

$$S(t) = 1 - R(t)/R_0(t) = \frac{(\rho_{1,1}/\gamma_{1,1} - 1/N)}{(1 - 1/N)} \tag{77}$$

is 1 for the completely synchronous state and 0 for the asynchronous state. We hereafter call $S(t)$ the *synchronization ratio*, which provides the degree of synchronous firings in the ensemble. We get $S = 0$ for $w/\beta^2 \to 0$, while $S = 1$ for $\beta^2/w \to 0$ [Eq. (57)].

III. CALCULATED RESULTS

We expect that our DMA equations given by Eqs. (20)–(27) may show bifurcation, synchronous and asynchronous states, as well as chaotic states. In this study, we pay our attention to the response of the FN neuron ensembles to a single spike input, $I^{(e)}(t)$ given by Eq. (3), which is applied to all neurons in the ensemble. We have adopted the parameters of $\theta = 0.5$, $\alpha = 0.1$, $\tau_r = 10$, $A = 0.10$, $t_{in} = 100$, and $T_w = 10$. Parameter values of w, β, and N will be explained shortly. We get the critical magnitude of $A_c = 0.0442$ below which firings of neuron defined by Eq. (58) cannot take place without noises ($\beta = 0$). We have adopted the value of $A = 0.10$ ($> A_c$) for the study of response to a suprathreshold input, related discussion being given in Sec. V.

DMA calculations have been made by solving Eqs. (20)–(27) by the fourth-order Runge-Kutta method with a time step of 0.01. Direct simulations have been performed by solving $2N$ DEs as given by Eqs. (1) and (2) by also using the fourth-order Runge-Kutta method with a time step of 0.01. Simulation results are the average of 100 trials, otherwise noticed. Initial values of variables are set to be $\mu_1 = \mu_2 = \gamma_{1,1} = \gamma_{1,1} = \gamma_{1,2} = \rho_{1,1} = \rho_{2,2} = \rho_{1,2} = 0$ in DMA calculations, and $x_i = y_i = 0$ for $i = 1$ to N in direct simulations. All calculated quantities are dimensionless.

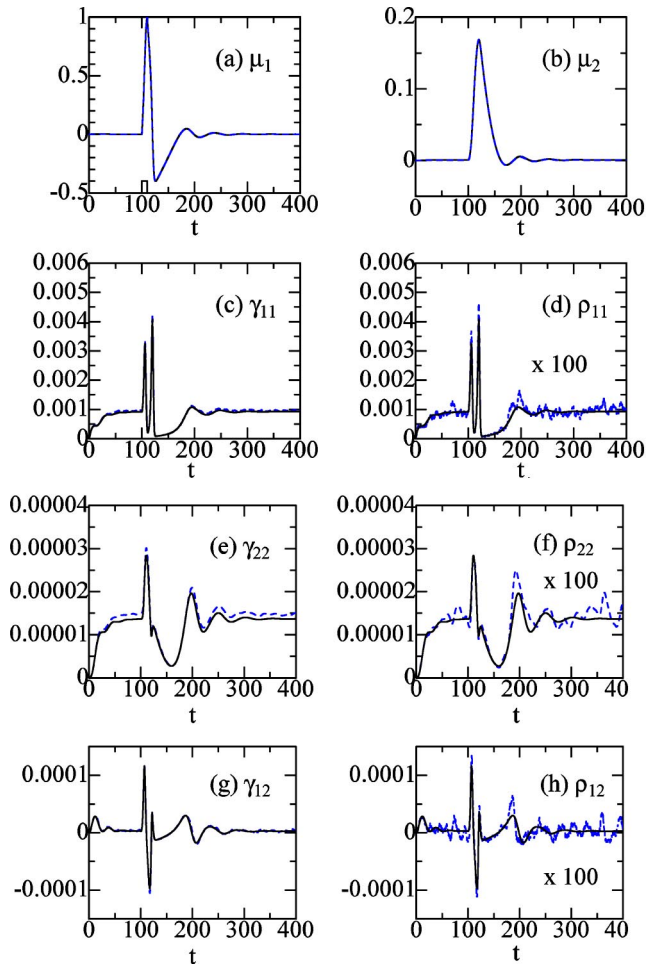

FIG. 1. Time courses of means, variances, and covariances calculated by DMA theory (solid curves) and simulations (dashed curves): (a) μ_1, (b) μ_2, (c) $\gamma_{1,1}$, (d) $\rho_{1,1}$, (e) $\gamma_{2,2}$, (f) $\rho_{2,2}$, (g) $\gamma_{1,2}$, and (h) $\rho_{1,2}$ for $A = 0.10$, $\beta = 0.01$, $w = 0.0$, and $N = 100$. Results of (d), (f), and (h) are multiplied by a factor of 100. The chain curve at the bottom of (a) expresses a single input spike, $I^{(e)}$, in Eq. (3) [see also Fig. 2(a)].

The time courses of means of μ_1 and μ_2 calculated with $\beta = 0.01$, $w = 0.0$, and $N = 100$ are shown in Figs. 1(a) and 1(b), respectively, where solid curves denote the results of DMA theory and dashed curves those of direct simulations. We note that μ_1 and μ_2 obtained by two methods are in very good agreement and they are indistinguishable. At the bottom of Fig. 1(a), an input spike is plotted [see also Fig. 2(a)]. States of neurons in an ensemble when an input spike is injected at $t = 100$ are randomized because noises have been already added since $t = 0$. Figures 1(c)–1(h) show the time courses of various variances and covariances. Agreements between the two methods are good for $\gamma_{1,1}$, $\rho_{1,1}$, $\gamma_{1,2}$, and $\rho_{1,2}$. There is a fairly good agreement for $\gamma_{2,2}$ and $\rho_{2,2}$. Comparing Figs. 1(c), 1(e), and 1(g) with 1(d), 1(f), and 1(h), respectively, we note that the relation given by Eq. (57), $\rho_{\kappa,\lambda} = \gamma_{\kappa,\lambda}/100$ valid for $w = 0$, is supported by simulations. Note that results in Figs. 1(d), 1(f), and 1(h) are multiplied by a factor of 100.

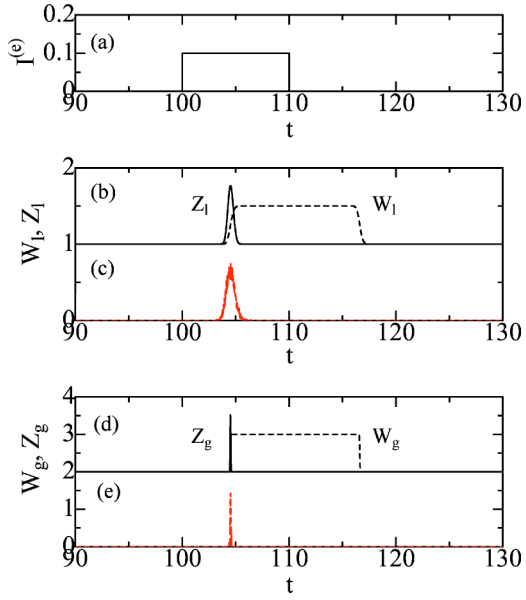

FIG. 2. Time courses of (a) $I^{(e)}$, (b) W_ℓ (the dashed curve) and Z_ℓ (the solid curve) in DMA theory, (c) Z_ℓ in simulations, (d) W_g (the dashed curve) and Z_g (the solid curve) in DMA theory, and (e) Z_g in simulations, for $A=0.10$, $\beta=0.01$, $w=0.0$, and $N=100$.

Figures 2(a) shows a single spike input, which is applied at $t=100$ with a duration of $T_w=10$. The solid curve in Fig. 2(b) express Z_ℓ, the firing probability of the local variable $x_i(t)$, which is a positive derivative of W_ℓ shown by the dashed curve [Eqs. (63) and (64)]. They are calculated for $\beta=0.01$, $w=0.0$, and $N=100$ in DMA theory. For a comparison, the simulation result for Z_ℓ is plotted in Fig. 2(c). Firings of neurons occur at $t_o \sim 104-105$ with a delay of about $4-5$. Fluctuations of firing times of local variables $\delta t_{o\ell}$ are 0.37 calculated by Eq. (66) in DMA theory, and 0.41 in simulations, which is the root-mean-square (rms) value of firing times defined by Eq. (58). In contrast, dashed and solid curves in Fig. 2(d) show W_g and Z_g, respectively, for the global variable $X(t)$ in DMA theory, while Fig. 2(e) shows Z_g obtained in simulations. Fluctuations in spike timings of the global variable are $\delta t_{og}=0.037$ calculated by Eq. (73) in DMA theory, and 0.041 in simulations which is the rms value of firing times defined by Eq. (71). These figures of δt_{og} for the global variable are ten times smaller than respective values of $\delta t_{o\ell}$ for the local variable.

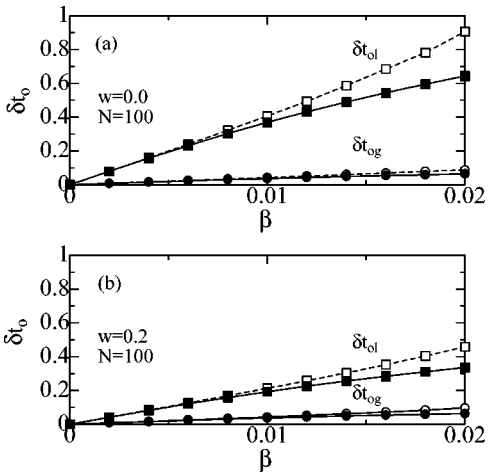

FIG. 3. (a) The β dependence of $\delta t_{o\ell}$ (squares) and δt_{og} (circles) for $w=0.0$ and (b) that for $w=0.2$ with $N=100$; filled symbols denoting results in DMA theory and open symbols those in simulations.

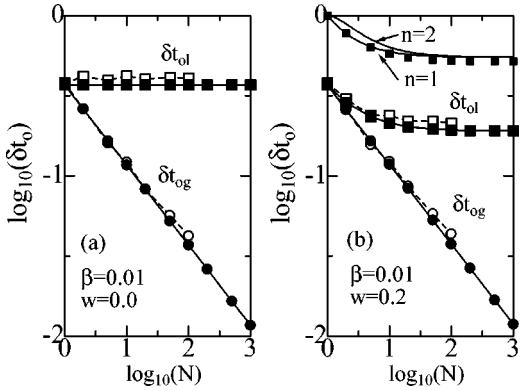

FIG. 4. Log-log plots of $\delta t_{o\ell}$ (squares) and δt_{og} (circles) against N for (a) $w=0.0$ and (b) $w=0.2$, filled symbols denoting results in DMA theory and open symbols those in simulations. Shown at the uppermost part in (b) are the DMA result (small, filled squares) and results with Eq. (E1) with $n=1$ and 2 (thin solid curves): they are shifted upward by 0.433 for the clarity of the figure (see text).

A. Noise-strength β dependence

We expect that as the noise strength is more increased, the distribution of membrane potentials is more wider and fluctuations of firing times are more increased. Filled squares in Fig. 3(a) show the β dependence of $\delta t_{o\ell}$ obtained by DMA theory [Eq. (66)] with $w=0.0$ and $N=100$, while open squares express the rms value of firing times obtained by simulations. The agreement between the two methods is fairly good. In contrast, filled circles in Fig. 3(a) show the β dependence of δt_{og} relevant to the global variable obtained by DMA theory [Eq. (73)] and open circles stand for RMS values of firing times in simulations. We note that δt_{og} is much smaller than $\delta t_{o\ell}$ although both δt_{og} and $\delta t_{o\ell}$ are proportional to β for weak noises under consideration. Figure 3(b) will be explained shortly in connection to the result of the w dependence.

B. Cluster-size N dependence

Filled squares in Fig. 4(a) show the N dependence of the local fluctuation of $\delta t_{o\ell}$ for $\beta=0.01$ and $w=0.0$, obtained by DMA theory, while open squares express that obtained by simulations. Simulations have not been performed for $N>100$ because of a limitation in our computer facility. We note that $\delta t_{o\ell}$ is independent of N because of no couplings ($w=0$). In contrast, filled circles in Fig. 4(a) show the N dependence of the global fluctuation of δt_{og} obtained by DMA theory, while open circles that by simulations. The relation, $\delta t_{og} \propto (1/\sqrt{N})$, holds as given by Eq. (75). Figure 4(b) for finite w will be discussed shortly.

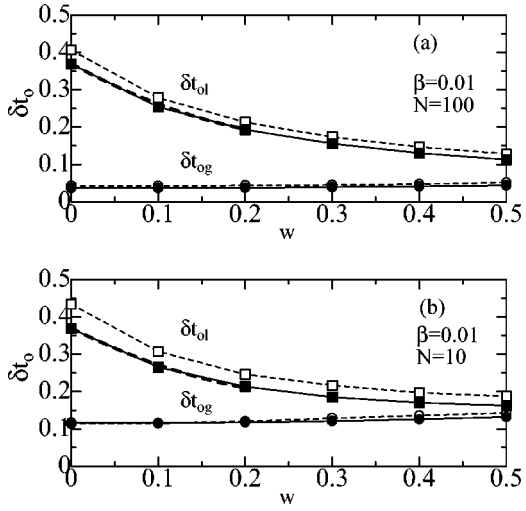

FIG. 5. The w dependence of $\delta t_{o\ell}$ (squares) and δt_{og} (circles) for (a) $N=100$ and (b) $N=10$ with $\beta=0.01$, filled symbols denoting results in DMA theory and open symbols those in simulations. Bold, dashed curves for $w\leqslant 0.2$ express Eq. (78) (see text).

C. Coupling-strength w dependence

So far, we have neglected the coupling w among neurons, which is now introduced. Filled squares in Fig. 3(b) show the β dependence of local fluctuations of $\delta t_{o\ell}$ calculated by DMA theory for $w=0.2$ and $N=100$, while open squares that obtained by simulations. Filled and open circles express global fluctuations of δt_{og} in the DMA theory and simulations, respectively. Comparing these results with those for $w=0.0$ shown in Fig. 3(a), we note that $\delta t_{o\ell}$ is much reduced as w is increased, although there is little change in δt_{og}.

This is more clearly seen in Fig. 5(a), which shows the w dependence of firing-time fluctuations. Filled squares in Fig. 5(a) show fluctuations of $\delta t_{o\ell}$ for the local variable obtained for $\beta=0.01$ and $N=100$ by the DMA theory, while open squares express those calculated by simulations. Filled and open circles in Fig. 5(a) show fluctuations of δt_{og} for the global variable obtained by the DMA theory and simulations, respectively. When w is increased, $\delta t_{o\ell}$ is considerably decreased, whereas δt_{og} is almost constant. Figure 5(b) shows a similar plot of the w dependence of firing times when the size of an ensemble is reduced to $N=10$. We note that δt_{og} for $N=10$ is 3.16 times larger than δt_{og} for $N=100$ because δt_{og} is proportional to $1/\sqrt{N}$.

Results obtained by DMA theory are analyzed in the Appendix E, where we get the expression for the w and N dependent $\delta t_{o\ell}$ given by [see Eq. (E1)]

$$\frac{\delta t_{o\ell}(w,N)}{\delta t_{o\ell}(0,1)} \sim 1-\left(\frac{1}{2}\right)\left(1-\frac{1}{N}\right)^{n}(a_1 w+a_2 w^2+\cdots), \tag{78}$$

where $n=1$, $\delta t_{o\ell}(0,1)=2.71$, $a_1=7.0$, and $a_2=-11.0$. Bold, dashed curves for $w\leqslant 0.2$ in Figs. 5(a) and 5(b) show the w dependence of $\delta t_{o\ell}$ for $N=100$ and 10, respectively, expressed by Eq. (78), which are in good agreement with results of DMA theory shown by filled squares.

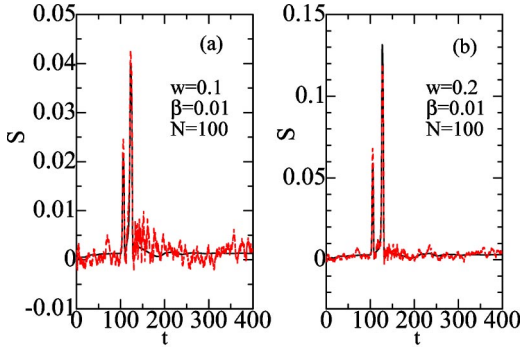

FIG. 6. The time course of synchronization ratio S for (a) $w=0.1$ and (b) $w=0.2$ with $\beta=0.01$ and $N=100$, the solid curve denoting results of DMA theory and the dashed curve those of simulations.

Log-log plots of Fig. 4(b) show the N dependence of $\delta t_{o\ell}$ (squares) and δt_{og} (circles) for $w=0.2$ and $N=100$, filled and open symbols denoting results of DMA and simulations, respectively. Although $\delta t_{og}\propto(1/\sqrt{N})$ as in the case of $w=0$ [Fig. 4(a)], $\delta t_{o\ell}$ shows the peculiar N dependence, which arises from the $(1-1/N)$ term in Eq. (78). The N dependence given by Eq. (78) with $n=1$ and 2 is shown by thin solid curves at the uppermost part in Fig. 4(b), which are shifted upward by 0.433 for a clarity of the figure. The result with $n=1$ is in better agreement with the result of DMA theory shown by small filled squares than that with $n=2$ (see Appendix E).

Couplings among neurons work to increase the synchronous dynamics and to suppress local fluctuations. Figures 6(a) and 6(b) show the time sequence of the synchronization ratio $S(t)$ defined by Eq. (77) for $w=0.1$ and $w=0.2$, respectively, with $\beta=0.01$ and $N=100$. Solid and dashed curves in Figs. 6(a) and 6(b) show results in DMA theory and simulations, respectively. Both results are in fairly good agreement. We note that $S(t)$ has two peaks at times when $\rho_{1,1}(t)$ also has double peaks [Fig. 1(d)]. The maximum value of $S(t)$ for $w=0.2$ is $S_{\max}=0.132$, which is larger than $S_{\max}=0.041$ for $w=0.1$. This trend is more clearly seen in Fig. 7, where the maximum magnitude of $S(t)$, $S_{\max}$, is plotted as a function of w for $N=10$, 20, 50, and 100. It is shown

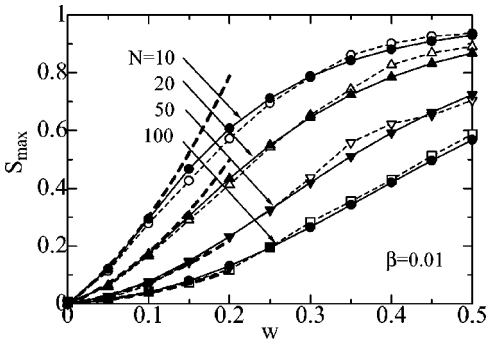

FIG. 7. The w dependence of the maximum of S, S_{max}, for $N=10$ (squares), $N=20$ (triangles), $N=50$ (inverted triangles), and $N=100$ (circles) with $\beta=0.01$, filled symbols denoting results of DMA theory and open symbols those of simulation. Bold, dashed curves for $w\leqslant 0.2$ express Eqs. (79)–(81) (see text).

that S_{max} is increased as the coupling strength is increased, as expected. Figure 7 also shows that the effect of coupling is more significant in ensembles with smaller N.

An analysis of the result obtained in DMA theory yields the expression for w- and N-dependent S_{max} given by [see Eq. (E8) in Appendix E]

$$S_{max}(w,N)=c_1 w+c_2 w^2+\cdots, \tag{79}$$

with

$$c_1=\left(\frac{1}{N}\right)\left(1-\frac{1}{N}\right)b_1, \tag{80}$$

$$c_2=\left(\frac{1}{N}\right)\left(1-\frac{1}{N}\right)\left[b_2+\left(1-\frac{1}{N}\right)^2 b_1^2\right], \tag{81}$$

where $b_1=22$ and $b_2=-290$. Bold, dashed curves for $w \leqslant 0.2$ in Fig. 7 show S_{max} expressed by Eqs. (79)–(81), which are in good agreement with results obtained in DMA theory shown by solid curves. If we define the coupling constant $w_m(N)$ for which S_{max} is, for example, 0.3 for a given N, we get $w_m(N)=0.101$, 0.147 0.237, and 0.322 for $N=10$, 20, 50, and 100, respectively, which lead to $w_m(N)/w_m(10)=1.0$, 1.46, 2.35, and 3.19, respectively, when $w_m(N)$ is normalized by $w_m(N=10)$. This suggests that we may get $w_m(N) \propto \sqrt{N}$. This arises from the fact that the relation: $S_{max} \propto w^2/N$ nearly holds for $S_{max}=0.3$, for which the contribution from the w^2 term is more considerable than that from the w term in Eqs. (79)–(81). Of course, it is not the case for much smaller value of S_{max}, for which the first term is more dominant than the second term.

Expressions of Eqs. (E1)–(E8) for w- and N dependence of fluctuations and the synchronization ratio, which are obtained based on the results calculated in DMA theory, are useful in a phenomenological sense. For example, in the case of *negative* (inhibitory) couplings, Eqs. (E1) and (E8) yield an increase in $\delta t_{o\ell}$ and a negative S, which are supported by numerical calculations with DMA theory and simulations (not shown). We have tried to extract coefficients a_1, a_2, b_1, and b_2 in Eqs. (E1)–(E8), by expanding Eqs. (20)–(27) in terms of w, but have not succeeded yet.

IV. DISCUSSIONS

It is possible to extend the DMA theory we proposed to a large FN neuron cluster that is divided into multiple M subclusters according to their functions. Dynamics of a single FN neuron i in a given subcluster m ($=1$ to M) that consists of N_m neurons is described by the nonlinear DEs given by

$$\frac{dx_i(t)}{dt}=F[x_i(t)]-cy_i(t)+I_i^{(c1)}(t)+I_i^{(c2)}(t) + I_m^{(e)}(t)+\xi_i(t), \tag{82}$$

$$\frac{dy_i(t)}{dt}=bx_i(t)-dy_i(t)+e \quad (i=1-N_m), \tag{83}$$

where x_i and y_i denote the fast (voltage) variable and slow (recovery) variable, respectively, $\xi_i(t)$ the Gaussian white noise with $\langle \xi_i(t)\rangle=0$ and $\langle \xi_i(t)\xi_j(t')\rangle=\beta^2\delta_{ij}\delta(t-t')$, the bracket $\langle\cdots\rangle$ denoting the average [57]. In Eq. (82), $I_i^{(c1)}(t)$ and $I_i^{(c2)}(t)$ are given by

$$I_i^{(c1)}(t)=\frac{w_{mm}}{N_m}\sum_{j\in m} G(x_j(t)), \tag{84}$$

$$I_i^{(c2)}(t)=\sum_{n(\neq m)}\left(\frac{w_{mn}}{N_n}\right)\sum_{k\in n} G(x_k(t)), \tag{85}$$

which express the couplings within the subcluster m with strength w_{mm}, and those between subclusters with strength w_{mn}, respectively, N_m the number of neurons in the subcluster m, and $G(x)$ is the sigmoid function. $I_m^{(e)}(t)$ stands for an external single spike input applied to all neurons in the subcluster m, as given by Eq. (3).

As in the Sec. IIA, we first define the global variables for the subcluster m by

$$X^m(t)=\frac{1}{N_m}\sum_{i\in m} x_i(t), \tag{86}$$

$$Y^m(t)=\frac{1}{N_m}\sum_{i\in m} y_i(t), \tag{87}$$

and their averages by [57]

$$\mu_1^m(t)=\langle X^m(t)\rangle, \tag{88}$$

$$\mu_2^m(t)=\langle Y^m(t)\rangle. \tag{89}$$

Next we define variances and covariances between local variables in the subcluster m, given by

$$\gamma_{1,1}^m=\frac{1}{N_m}\sum_{i\in m}\langle(\delta x_i^m)^2\rangle, \tag{90}$$

$$\gamma_{2,2}^m=\frac{1}{N_m}\sum_{i\in m}\langle(\delta y_i^m)^2\rangle, \tag{91}$$

$$\gamma_{1,2}^m=\frac{1}{N_m}\sum_{i\in m}\langle(\delta x_i^m \delta y_i^m)\rangle, \tag{92}$$

and those between global variables in the subcluster m, given by

$$\rho_{1,1}^m=\langle(\delta X^m)^2\rangle, \tag{93}$$

$$\rho_{2,2}^m=\langle(\delta Y^m)^2\rangle, \tag{94}$$

$$\rho_{1,2}^m=\langle(\delta X^m \delta Y^m)\rangle, \tag{95}$$

where $\delta x_i^m=x_i(t)-\mu_1^m(t)$, $\delta y_i^m=y_i(t)-\mu_2^m(t)$, $\delta X^m=X^m(t)-\mu_1^m(t)$, and $\delta Y^m=Y^m(t)-\mu_2^m(t)$. Covarinaces between variables belonging to different subclusters are not taken into account. As in the single ensemble case discussed

in Sec. II A, we assume a weak noise and the Gaussian distribution of state variables adopting the mean-field approximation. After some manipulations, we get the following DEs:

$$\frac{d\mu_1^m}{dt} = f_0^m + f_2^m \gamma_{1,1}^m - c\mu_2^m + w_{mm}\left(1 - \frac{1}{N_m}\right) U_{om} + \sum_{n(\neq m)} w_{mn} U_{0n} + I_m^{(e)}(t), \tag{96}$$

$$\frac{d\mu_2^m}{dt} = b\mu_1^m - d\mu_2^m + e, \tag{97}$$

$$\frac{d\gamma_{1,1}^m}{dt} = 2[(f_1^m + 3f_3^m \gamma_{1,1}^m)\gamma_{1,1}^m - c\gamma_{1,2}^m] + 2w_{mm}\left(\rho_{1,1}^m - \frac{\gamma_{1,1}^m}{N_m}\right) U_{1m} + 2\sum_{n(\neq m)} w_{mn}\rho_{1,1}^n U_{1n} + \beta^2, \tag{98}$$

$$\frac{d\gamma_{2,2}^m}{dt} = 2(b\gamma_{1,2}^m - d\gamma_{2,2}^m), \tag{99}$$

$$\frac{d\gamma_{1,2}^m}{dt} = b\gamma_{1,1}^m + (f_1^m + 3f_3^m \gamma_{1,1}^m - d)\gamma_{1,2}^m - c\gamma_{2,2}^m + w_{mm}\left(\rho_{1,2}^m - \frac{\gamma_{1,2}^m}{N_m}\right) U_{1m} + \sum_{n(\neq m)} w_{mn}\rho_{1,2}^n U_{1n}, \tag{100}$$

$$\frac{d\rho_{1,1}^m}{dt} = 2[(f_1^m + 3f_3^m \gamma_{1,1}^m)\rho_{1,1}^m - c\rho_{1,2}^m] + 2w_{mm}\left(1 - \frac{1}{N_m}\right)\rho_{1,1}^m U_{1m} + \frac{\beta^2}{N_m}, \tag{101}$$

$$\frac{d\rho_{2,2}^m}{dt} = 2(b\rho_{1,2}^m - d\rho_{2,2}^m), \tag{102}$$

$$\frac{d\rho_{1,2}^m}{dt} = b\rho_{1,1}^m + (f_1^m + 3f_3^m \gamma_{1,1}^m - d)\rho_{1,2}^m - c\rho_{2,2}^m + w_{mm}\left(1 - \frac{1}{N_m}\right)\rho_{1,2}^m U_{1m}, \tag{103}$$

with

$$U_{0m} = g_o^m + g_2^m \gamma_{1,1}^m, \tag{104}$$

$$U_{1m} = g_1^m + 3g_3^m \gamma_{1,1}^m, \tag{105}$$

where $f_\ell^m = (1/\ell!)F^{(\ell)}(\mu_1^m)$ and $g_\ell^m = (1/\ell!)G^{(\ell)}(\mu_1^m)$. Now we have to solve $8M$-dimensional deterministic DEs [Eqs. (96)–(103)], which are more amenable than $2NM$ stochastic DEs.

When a given cluster can be divided into excitatory and inhibitory subgroups and when variance and covariance terms in Eqs. (96)–(103) are neglected, we get

$$\frac{d\mu_1^E}{dt} = f_0^E - c\mu_2^E + w_{EE}U_E + w_{EI}U_I + I_E^{(e)}(t), \tag{106}$$

$$\frac{d\mu_2^E}{dt} = b\mu_1^E - d\mu_2^e + e, \tag{107}$$

$$\frac{d\mu_1^I}{dt} = f_0^I - c\mu_2^I + w_{II}U_I + w_{IE}U_E + I_I^{(e)}(t), \tag{108}$$

$$\frac{d\mu_2^I}{dt} = b\mu_1^I - d\mu_2^I + e, \tag{109}$$

where the suprascripts E and I stand for the excitatory and inhibitory clusters, respectively. This corresponds to the result of Wilson and Cowan [58]. Then our DMA theory given by Eqs. (96)–(103) may be regarded as a generalized version of the Wilson-Cowan theory including fluctuations of local and global variables.

The fraction of firings of neurons in the subcluster m is given by

$$Z_{om}(t) = \phi\left(\frac{\theta - \mu_1^m}{\sigma_{\ell m}}\right)\frac{d}{dt}\left(\frac{\mu_1^m}{\sigma_{\ell m}}\right)\Theta(\dot{\mu}_1^m), \tag{110}$$

with

$$\sigma_{\ell m} = \sqrt{\gamma_{1,1}^m}. \tag{111}$$

When we expand $\mu_1^m(t)$ in Eq. (110) around t_{om}^*, where $\mu_1^m(t_{om}^*) = \theta$, it becomes

$$Z_{om}(t) \sim \phi\left(\frac{t - t_{om}^*}{\delta t_{om}}\right)\frac{d}{dt}\left(\frac{\mu_1^m}{\sigma_{\ell m}}\right)\Theta(\dot{\mu}_1^m), \tag{112}$$

with

$$\delta t_{om} = \frac{\sigma_{\ell m}}{\dot{\mu}_1^m}, \tag{113}$$

where μ_1^m, $\dot{\mu}_1^m$, and $\sigma_{\ell m}$ are evaluated at $t = t_{om}^*$. This shows that most of the firing times of a given subcluster m are located in the range given as

$$t_{om} \in [t_{om}^* - \delta t_{om},\ \ t_{om}^* + \delta t_{om}]. \tag{114}$$

The synchronization ratio of a given subcluster m is given by

$$S_m(t) = \frac{\rho_{1,1}^m/\gamma_{1,1}^m - 1/N_m}{1 - 1/N_m}, \tag{115}$$

which is 0 and 1 for completely asynchronous and synchronous states, respectively.

We have performed model calculations, assuming M $(=10)$ subclusters, each of which consists of $N_m(=N)$ neu-

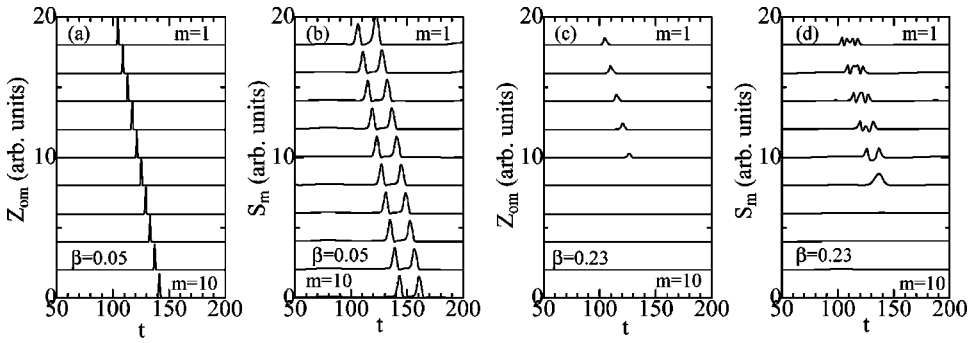

FIG. 8. Time courses of (a) Z_{om} and (b) S_m for $\beta=0.05$ and those of (c) Z_{om} and (d) S_m for $\beta=0.23$ calculated with $w_1=w_2=0.1$, $N=100$, and $M=10$ by DMA theory.

rons. They are connected by feed-forward intersubcluster coupling given by $w_{mn}=w_2\delta_{nm-1}$, which is allowed to be different from the intrasubcluster coupling given by $w_{mm}=w_1$ for all m. A single spike input given by Eq. (3) is applied only to the first subcluster ($m=1$), and an output of a subcluster m is subsequently forwarded to the next subcluster $m+1$. This is conceptually similar to the synfire chain [59]. When w_2 is too small, signals cannot propagate through subclusters. The critical value of the intersubcluster coupling w_{2c}, below which a spike cannot propagate through subclusters, is $w_{2c}=0.064$, 0.028, and 0.020 for $w_1=0.0$, 0.1, and 0.2, respectively, with $\beta=0.0$ and $N=100$.

Figure 8(a) shows the time course of $Z_{om}(t)$ calculated in the DMA theory with $\beta=0.05$, $w_1=w_2=0.1$, and $N=100$. Signals propagate through subclusters with $\delta t_{om}\simeq 0.8$ for all m. The result is in good agreement with that obtained in direct simulations (not shown). Synchronization ratios $S_m(t)$ shown in Fig. 8(b) have double peaks [see Figs. 6(a) and 6(b)]. The maximum value of $S_m(t)$, for example, is 0.022 for $m=1$ at $t=122.2$.

In contrast, Fig. 8(c) shows the time course of $Z_{om}(t)$ for the increased noise intensity of $\beta=0.23$, which shows that signals cannot propagate, dying out at the sixth subcluster. In this case, the agreement of DMA results with simulations is not satisfactory. Synchronization ratios $S_m(t)$ for $\beta=0.23$ shown in Fig. 8(d) have multiple peaks for $1\leqslant m\leqslant 4$, double peaks for $m=5$, a single peak for $m=6$, and it disappears for $m>6$.

Figure 9(a) shows the m dependence of local fluctuations δt_{om} for various β with $w_1=w_2=0.1$ and $N=100$. We note that δt_{om} is almost constant for $\beta=0.05$ and 0.10. In the case of $\beta=0.23$, however, δt_{om} is divergently increased at $m=5$. This behavior is not changed when we adopt a different set of parameters. Figure 9(b) shows a similar plot of δt_{om} as a function of m for $w_1=0.0$, $w_2=0.1$, and $N=100$. Signals propagate with $\delta t_{om}=0.04$ and 0.12 for $\beta=0.01$ and 0.05, respectively. For $\beta=0.09$, however, a spike dies out at $m=8$.

Figure 10 shows the w_1 dependence of the critical noise strength β_c, above which signals cannot propagate. We get $\beta_c=0.09$ and 0.23 for $w_1=0.0$ and 0.1, respectively, for $N=100$ as discussed above. When w_1 is set to be 0.2, β_c becomes 0.38 for $N=100$. We note that β_c is almost linearly increased by increasing w_1. Figure 10 also shows that the critical value of β_c becomes larger as the size of subcluster (N) is larger.

V. CONCLUSIONS

We have proposed a DMA theory for stochastic FN neuron ensembles, in which means, variances, and covariances of *local* and *global* variables are taken into account. Our DMA theory, which assumes weak noises and the Gaussian distribtuion of state variables with the mean-field approximation, has been derived in various ways: (1) equations of motions for means, variances, and covariances of local and global variables (Sec. II A), (2) a reduction in the number of moments in the moment method with the mean-field ap-

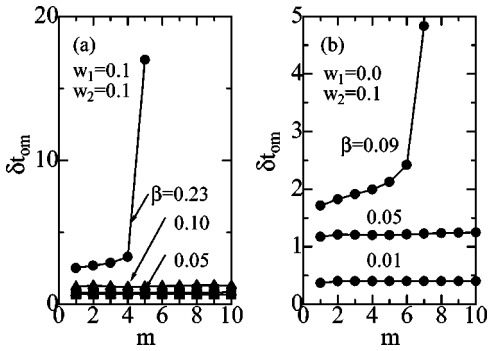

FIG. 9. δt_{om} as a function of m for (a) $w_1=w_2=0.1$ and (b) $w_1=0.1$ and $w_2=0.0$ with $N=100$ and $M=10$.

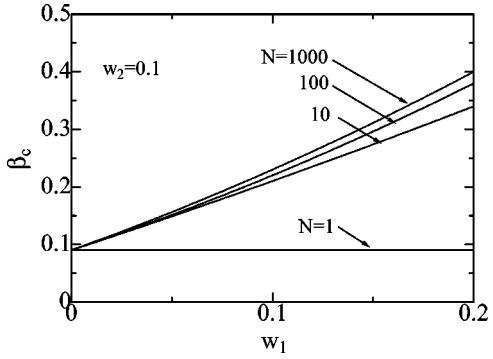

FIG. 10. The w_1 dependence of β_c for various N values with $w_2=0.1$.

proximation (Sec. II B), and (3) a single-site self-consistent approximation to the moment method [Sec. II C]. In particular, results obtained from the second-order moment method [43] have been shown to exactly agree with those of DMA. Calculated results based on DMA theory are in good agreement with those obtained by direct simulations for weak noises. When the noise intensity becomes stronger, the state-variable distribution more deviates from the Gaussian form (see Fig. 3 of Ref. [47]), and the agreement of results of DMA theory with those of simulations becomes worse. Nevertheless, our DMA theory is expected to be meaningful for qualitative or semiquantitative discussion on the properties of neuron ensembles or clusters. It is possible to regard nonlinear DEs given by Eqs. (20)–(27) [or Eqs. (96)–(103)] as the *mean-field FN model* for neuron ensembles or clusters. We hope that our DMA theory may play a role of the molecular-field (Weiss) theory in magnetism [55]: the Weiss theory provides a clear physical picture on various magnetic properties despite some disadvantages such that it yields too-high critical (Curie) temperature, wrong critical indices, and wrong temperature dependence for magnetization at low temperatures. Our DMA theory may be applied to a general conductance-based nonlinear systems. When we consider an ensemble of N-unit neurons, each of which is described by K-variable nonlinear DEs, the number of the deterministic DEs in DMA is $N_{eq}=K+K(K+1)=K(K+2)$ independent of N. For an ensemble of N *HH* neurons ($K=4$), for example, DMA yields $N_{eq}=24$ which is more amenable than original $4N$ stochastic equations [60]. Furthermore, our DMA theory based on moments of local and global variables can be applied to more general stochastic systems besides neural networks [61].

In summary, we have developed a semianalytical DMA theory for FN neuron ensembles. In order to show the feasibility of the DMA theory, we have studied the response of ensembles of FN neurons to a single spike input. The result is summarized as follows.

(i) The spike timing precision of the global variable is much improved by increasing the ensemble size, even when there is no coupling among constituent neurons.

(ii) By increasing the coupling strength, the spike transmission is enhanced by the synchronous response.

(iii) The spike propagation with a fairly precise timing is possible in large-scale clusters when the noise strength is moderate.

The origin of the item (i) is the same as that yielding the central-limit theorem. The couplings suppress local fluctuations and increase the synchronization ratio [Eq. (77)]. Items (i) and (ii) are consistent with the results reported previously [30–35]. The item (iii) agrees with the result of recent simulations for synfire chains, each layer of which consists of 100 IF neurons [62]. Items (i)–(iii) are beneficial to the population temporal-code hypothesis mentioned in the Introduction. Although calculations reported in this paper have been limited to suprathreshold inputs, it is possible to study the response to subthreshold inputs with the use of DMA theory. We may investigate combined effects of white noises and the heterogeneity in model parameters, which have been intensively studied in recent years [63]. Such calculations are in progress and will be reported in a separate paper.

ACKNOWLEDGMENTS

The author would like to express his sincere thanks to Professor Hideo Nitta for a critical reading of the manuscript. This work was partly supported by a Grant-in-Aid for Scientific Research from the Japanese Ministry of Education, Culture, Sports, Science, and Technology.

APPENDIX A: DERIVATION OF EQS. (20)–(27) AND EQS. (32)–(36)

From Eqs. (9)–(13), we get DEs for the deviations of δx_i and δy_i of the neuron i, given by

$$\frac{d\,\delta x_i}{dt}=f_1\delta x_i+f_2(\,\delta x_i^2-\gamma_{1,1})+f_3\delta x_i^3-c\,\delta y_i+\xi_i+\delta I_i^{(c)}, \tag{A1}$$

$$\frac{d\,\delta y_i}{dt}=b\,\delta x_i-d\,\delta y_i, \tag{A2}$$

with

$$\delta I_i^{(c)}=w\left(\frac{g_1}{N}\sum_{j(\neq i)}\delta x_j+g_2\left[\frac{1}{N}\sum_{j(\neq i)}\delta x_j^2-\left(1-\frac{1}{N}\right)\gamma_{1,1}\right]+\frac{g_3}{N}\sum_{j(\neq i)}\delta x_j^3\right). \tag{A3}$$

The differential equations for the variances and covariances are given by

$$\begin{aligned}\frac{d\gamma_{\kappa,\lambda}}{dt}&=\frac{d}{dt}\left(\frac{1}{N}\right)\sum_i\langle[(\delta x_i^2)\delta_{\kappa 1}\delta_{\lambda 1}+(\delta x_i\delta y_i)\delta_{\kappa 1}\delta_{\lambda 2}\\&\quad+(\delta y_i^2)\delta_{\kappa 2}\delta_{\lambda 2}]\rangle,\\&=\frac{1}{N}\sum_i\left\langle\left\{2\left[\delta x_i\left(\frac{d\,\delta x_i}{dt}\right)\right]\delta_{\kappa 1}\delta_{\lambda 1}+\left[\delta y_i\left(\frac{d\,\delta x_i}{dt}\right)+\delta x_i\left(\frac{d\,\delta y_i}{dt}\right)\right]\delta_{\kappa 1}\delta_{\lambda 2}+2\left[\delta y_i\left(\frac{d\,\delta y_i}{dt}\right)\right]\delta_{\kappa 2}\delta_{\lambda 2}\right\}\right\rangle,\end{aligned} \tag{A4}$$

$$\begin{aligned}\frac{d\rho_{\kappa,\lambda}}{dt}&=\frac{d}{dt}\left(\frac{1}{N^2}\right)\sum_i\sum_j\langle[(\delta x_i\delta x_j)\delta_{\kappa 1}\delta_{\lambda 1}\\&\quad+(\delta x_i\delta y_j)\delta_{\kappa 1}\delta_{\lambda 2}+(\delta y_i\delta y_j)\delta_{\kappa 2}\delta_{\lambda 2}]\rangle\\&=\frac{1}{N^2}\sum_i\sum_j\left\langle\left\{2\left[\delta x_i\left(\frac{d\,\delta x_j}{dt}\right)\right]\delta_{\kappa 1}\delta_{\lambda 1}+\left[\delta y_i\left(\frac{d\,\delta x_j}{dt}\right)+\delta x_i\left(\frac{d\,\delta y_j}{dt}\right)\right]\delta_{\kappa 1}\delta_{\lambda 2}+2\left[\delta y_i\left(\frac{d\,\delta y_j}{dt}\right)\right]\delta_{\kappa 2}\delta_{\lambda 2}\right\}\right\rangle,\end{aligned} \tag{A5}$$

In the process of the calculation using Eqs. (20)–(27), we have adopted the following Gaussian decoupling and mean-field approximations.

(1) The fourth-order variances are assumed to be [47]

$$\frac{1}{N}\sum_i \langle \delta x_i^4 \rangle \simeq 3\ \gamma_{1,1}\gamma_{1,1}, \tag{A6}$$

$$\frac{1}{N}\sum_i \langle \delta x_i^3 \delta y_i \rangle \simeq 3\ \gamma_{1,1}\gamma_{1,2}, \tag{A7}$$

and

$$\frac{1}{N^2}\sum_i \sum_j \langle \delta x_i \delta x_j^3 \rangle \simeq 3\gamma_{1,1}\rho_{1,1}, \tag{A8}$$

$$\frac{1}{N^2}\sum_i \sum_j \langle \delta y_i \delta x_j^3 \rangle \simeq 3\gamma_{1,1}\rho_{1,2}, \tag{A9}$$

other fourth-order terms being set to zero.

(2) The third-order variances and terms higher than fourth order are neglected,

Calculations of means, variances, and covariances given by Eqs. (32)–(36) in the moment method are similarly performed to get Eqs. (37)–(41) if we read as $m_1^i \to \mu_1$, $m_2^i \to \mu_2$, $\Delta x_i \to \delta x_i$, and $\Delta y_i \to \delta y_i$ for the calculation in DMA theory presented above.

APPENDIX B: COMPARISON OF DMA WITH THE MOMENT METHOD

With the use of Eqs. (37)–(41) and Eqs. (44)–(46), DEs for $d\overline{\mu}_\kappa/dt$, $d\overline{\gamma}_{\kappa,\lambda}/dt$, and $d\overline{\rho}_{\kappa,\lambda}/dt$ are given by (bars are neglected)

$$\frac{d\mu_1}{dt} = f_0 + f_2\gamma_{1,1} - c\mu_2 + w\left(1-\frac{1}{N}\right)(g_0 + g_2\gamma_{1,1}) + I^{(e)}(t), \tag{B1}$$

$$\frac{d\mu_2}{dt} = b\mu_1 - d\mu_2 + e, \tag{B2}$$

$$\frac{d\gamma_{1,1}}{dt} = 2(f_1\gamma_{1,1} - c\gamma_{1,2}) + 2w\, g_1\left(\rho_{1,1} - \frac{\gamma_{1,1}}{N}\right) + \beta^2 + 6f_3\left(\frac{1}{N}\right)\sum_i D_{1,1}^{i,i}D_{1,1}^{i,i} + 6wg_3\left(\frac{1}{N^2}\right)\sum_i \sum_k [D_{1,1}^{k,k}C_{1,1}^{i,k} - D_{1,1}^{i,i}D_{1,1}^{i,i}\delta_{ik}], \tag{B3}$$

$$\frac{d\gamma_{2,2}}{dt} = 2(b\gamma_{1,2} - d\gamma_{2,2}), \tag{B4}$$

$$\frac{d\gamma_{1,2}}{dt} = b\gamma_{1,1} + (f_1 - d)\gamma_{1,2} - c\gamma_{2,2} + w\, g_1\left(\rho_{1,2} - \frac{\gamma_{1,2}}{N}\right) + 3f_3\left(\frac{1}{N}\right)\sum_i D_{1,1}^{i,i}D_{1,2}^{i,i} + 6wg_3\left(\frac{1}{N^2}\right)\sum_i \sum_k [D_{1,1}^{k,k}C_{1,2}^{i,k} - D_{1,1}^{i,i}D_{1,2}^{i,i}\delta_{ik}], \tag{B5}$$

$$\frac{d\rho_{1,1}}{dt} = 2(f_1\rho_{1,1} - c\rho_{1,2}) + 2w\left(1-\frac{1}{N}\right)g_1\rho_{1,1} + \frac{\beta^2}{N} + 6f_3\left(\frac{1}{N^2}\right)\sum_i \sum_j D_{1,1}^{i,i}C_{1,1}^{i,j} + 6wg_3\left(\frac{1}{N^3}\right)\sum_i \sum_j \sum_{k(\neq i)} D_{1,1}^{k,k}C_{1,1}^{j,k}, \tag{B6}$$

$$\frac{d\rho_{2,2}}{dt} = 2(b\rho_{1,2} - d\rho_{2,2}), \tag{B7}$$

$$\frac{d\rho_{1,2}}{dt} = b\rho_{1,1} + (f_1 - d)\rho_{1,2} - c\rho_{2,2} + w\left(1-\frac{1}{N}\right)g_1\rho_{1,2} + 3f_3\left(\frac{1}{N^2}\right)\sum_i \sum_j D_{1,1}^{i,i}C_{1,2}^{i,j} + 3wg_3\left(\frac{1}{N^3}\right)\sum_i \sum_j \sum_{k(\neq i)} D_{1,1}^{k,k}C_{1,2}^{j,k}, \tag{B8}$$

where $D_{\kappa,\lambda}^{i,i} = C_{\kappa,\lambda}^{i,i} + d_{\kappa,\lambda}$, and $d_{\kappa,\lambda}$ is given by Eqs. (47) and (48). In deriving Eqs. (B1)–(B8), we employ expressions given by

$$f_0^i = f_0 + f_1\delta m_1^i + f_2(\delta m_1^i)^2 + f_3(\delta m_1^i)^3 + \cdots, \tag{B9}$$

$$f_1^i = f_1 + 2f_2\delta m_1^i + 3f_3(\delta m_1^i)^2 + \cdots, \tag{B10}$$

$$f_2^i = f_2 + 3f_3\delta m_1^i + \cdots, \tag{B11}$$

and corresponding ones for g_0^i, g_1^i, and g_2^i in Eqs. (42) and (43). Furthermore, we adopt DEs for $d\,\delta m_1^i/dt$ and $d\,\delta m_2^i/dt$ given by

$$\frac{d\,\delta m_1^i}{dt} = f_1\delta m_1^i + f_2(D_{1,1}^{i,i} - \gamma_{1,1}) + f_3[3C_{1,1}^{i,i} + (\delta m_1^i)^2]\delta m_1^i - c\ \delta m_2^i + \frac{w}{N}\sum_{k(\neq i)}\{g_1\delta m_1^k + g_2(D_{1,1}^{k,k} - \gamma_{1,1}) + g_3[3C_{1,1}^{k,k} + (\delta m_1^k)^2]\delta m_1^k\}, \tag{B12}$$

$$\frac{d\,\delta m_2^i}{dt} = b\,\delta m_1^i - d\ \delta m_2^i, \tag{B13}$$

and the Gasussin approximation given by

$$\frac{1}{N}\sum_i (\delta m_\kappa^i)^3 \delta m_\lambda^i \simeq 3 d_{\kappa,\kappa} d_{\kappa,\lambda}. \tag{B14}$$

We note that DEs for μ_1, μ_2, $\gamma_{2,2}$, and $\rho_{2,2}$ given by Eqs. (B1), (B2), (B4), and (B7) agree with those in DMA given by Eqs. (20), (21), (23), and (26), respectively. In contrast, although the *second-order* moment terms in DEs for $\gamma_{1,1}$, $\gamma_{1,2}$, $\rho_{1,1}$, and $\rho_{1,2}$ given by Eqs. (B3), (B5), (B6), and (B8) agree with those in DMA given by Eqs. (22), (24), (25), and (27), respectively, their *fourth-order* moment terms with f_3 and g_3 reduce to the corresponding terms in DMA when we adopt the mean-field approximations as given by

$$\frac{1}{N}\sum_i f_3 D_{1,1}^{i,i} D_{1,1}^{i,i} \simeq f_3 \gamma_{1,1}\left(\frac{1}{N}\right)\sum_i D_{1,1}^{i,i} = f_3 \gamma_{1,1}\gamma_{1,1}, \tag{B15}$$

$$\frac{1}{N^2}\sum_i \sum_k g_3 D_{1,1}^{k,k} C_{1,1}^{i,k} \simeq g_3 \gamma_{1,1}\left(\frac{1}{N^2}\right)\sum_i \sum_k C_{1,1}^{i,k} = g_3 \gamma_{1,1}\rho_{1,1}, \tag{B16}$$

with which Eqs. (B3), (B5), (B6), and (B8) fully agree with Eqs. (22), (24), (25), and (27), respectively. It is noted that Eqs. (B14)–(B16) are similar to Eqs. (A6)–(A9).

1. $N=1$ case

For a single neuron ($N=1$), Eqs. (B1)–(B8) reduce to

$$\frac{d\mu_1}{dt} = f_0 + f_2 \gamma_{1,1} - c\mu_1 + I^{(e)}(t), \tag{B17}$$

$$\frac{d\mu_2}{dt} = b\mu_1 - d\mu_2 + e, \tag{B18}$$

$$\frac{d\gamma_{1,1}}{dt} = 2(f_1 \gamma_{1,1} + 3 f_3 \gamma_{1,1}^2 - c\gamma_{1,2}) + \beta^2, \tag{B19}$$

$$\frac{d\gamma_{2,2}}{dt} = 2(b\gamma_{1,2} - d\gamma_{2,2}), \tag{B20}$$

$$\frac{d\gamma_{1,2}}{dt} = b\gamma_{1,1} + (f_1 - d)\gamma_{1,2} + 3 f_3 \gamma_{1,1}\gamma_{1,2} - c\gamma_{2,2}, \tag{B21}$$

$$\rho_{\kappa,\lambda} = \gamma_{\kappa,\lambda}. \tag{B22}$$

Equations (B17)–(B22) show that results of the moment method of Rodriguez and Tuckwell (RT) [44] and Tanabe and Pakdaman (TP) [47] agree with those of DMA with the relations: $\mu_\kappa = m_\kappa$ and $\gamma_{\kappa,\lambda} = \rho_{\kappa,\lambda} = C_{\kappa,\lambda}^{1,1}$. In RT, the fourth-order terms which appear in the process of calculating $d\gamma_{1,1}/dt$ and $d\gamma_{1,2}/dt$ in Eqs. (B19) and (B21) are assumed to be zero, whereas in TP, they are assumed to be given by Eqs. (A6) and (A7).

2. $N=2$ case

As mentioned above, expressions of μ_1, μ_2, $\gamma_{2,2}$, and $\rho_{2,2}$ for a pair of neuron ensemble ($N=2$) derived from the moment method agree with the DMA results. Expressions of $\gamma_{1,1}$, $\gamma_{1,2}$, $\rho_{1,1}$, and $\rho_{1,2}$ given by Eqs. (B3), (B5), (B6), and (B8) for $N=2$ become

$$\begin{aligned}\frac{d\gamma_{1,1}}{dt} &= 2(f_1\gamma_{1,1} - c\gamma_{1,2}) + 2w\, g_1\left(\rho_{1,1} - \frac{\gamma_{1,1}}{2}\right) + \beta^2 \\ &\quad + 3 f_3[D_{1,1}^{1,1}D_{1,1}^{1,1} + D_{1,1}^{2,2}D_{1,1}^{2,2}] + \left(\frac{3}{2}\right)w \\ &\quad \times g_3[D_{1,1}^{1,1}(C_{1,1}^{1,1} - D_{1,1}^{1,1}) + D_{1,1}^{2,2}(C_{1,1}^{2,2} - D_{1,1}^{2,2}) \\ &\quad + D_{1,1}^{2,2}D_{1,1}^{1,2} + D_{1,1}^{1,1}D_{1,1}^{2,1}],\end{aligned} \tag{B23}$$

$$\begin{aligned}\frac{d\gamma_{1,2}}{dt} &= b\gamma_{1,1} + (f_1 - d)\gamma_{1,2} - c\gamma_{2,2} + w\, g_1\left(\rho_{1,2} - \frac{\gamma_{1,2}}{2}\right) \\ &\quad + \left(\frac{3}{2}\right) f_3[D_{1,1}^{1,1}D_{1,2}^{1,1} + D_{1,1}^{2,2}D_{1,2}^{2,2}] + \left(\frac{3}{2}\right)w \\ &\quad \times g_3[D_{1,1}^{1,1}(C_{1,2}^{1,1} - D_{1,2}^{1,1}) + D_{1,1}^{2,2}(C_{1,2}^{2,2} - D_{1,2}^{2,2}) \\ &\quad + D_{1,1}^{2,2}D_{1,2}^{1,2} + D_{1,1}^{1,1}D_{1,2}^{2,1}],\end{aligned} \tag{B24}$$

$$\begin{aligned}\frac{d\rho_{1,1}}{dt} &= 2(f_1\rho_{1,1} - c\rho_{1,2}) + 2w\left(\frac{1}{2}\right)g_1\rho_{1,1} + \frac{\beta^2}{2} \\ &\quad + \left(\frac{3}{2}\right) f_3[D_{1,1}^{1,1}(C_{1,1}^{1,1} + C_{1,1}^{1,2}) + D_{1,1}^{2,2}(C_{1,1}^{2,1} + C_{1,1}^{2,2})] \\ &\quad + \left(\frac{3}{4}\right) w g_3[D_{1,1}^{2,2}(C_{1,1}^{1,2} + C_{1,1}^{2,2}) + D_{1,1}^{1,1}(C_{1,1}^{1,1} + C_{1,1}^{2,1})],\end{aligned} \tag{B25}$$

$$\begin{aligned}\frac{d\rho_{1,2}}{dt} &= b\rho_{1,1} + (f_1 - d)\rho_{1,2} - c\rho_{2,2} + w\left(\frac{1}{2}\right)g_1\rho_{1,2} \\ &\quad + \left(\frac{3}{4}\right) f_3[D_{1,1}^{1,1}(C_{1,2}^{1,1} + C_{1,2}^{1,2}) + D_{1,1}^{2,2}(C_{1,2}^{2,1} + C_{1,2}^{2,2})] \\ &\quad + \left(\frac{3}{8}\right) w g_3[D_{1,1}^{2,2}(C_{1,2}^{1,2} + C_{1,2}^{2,2}) + D_{1,1}^{1,1}(C_{1,2}^{1,1} + C_{1,2}^{2,1})].\end{aligned} \tag{B26}$$

Adopting the mean-field approximation as given by Eqs. (B15) and (B16), we get the following results obtained in DMA:

$$\frac{d\mu_1}{dt} = f_0 + f_2\gamma_{1,1} - c\mu_2 + \left(\frac{1}{2}\right)w\, U_0 + I^{(e)}(t), \tag{B27}$$

$$\frac{d\mu_2}{dt} = b\mu_1 - d\mu_2 + e, \tag{B28}$$

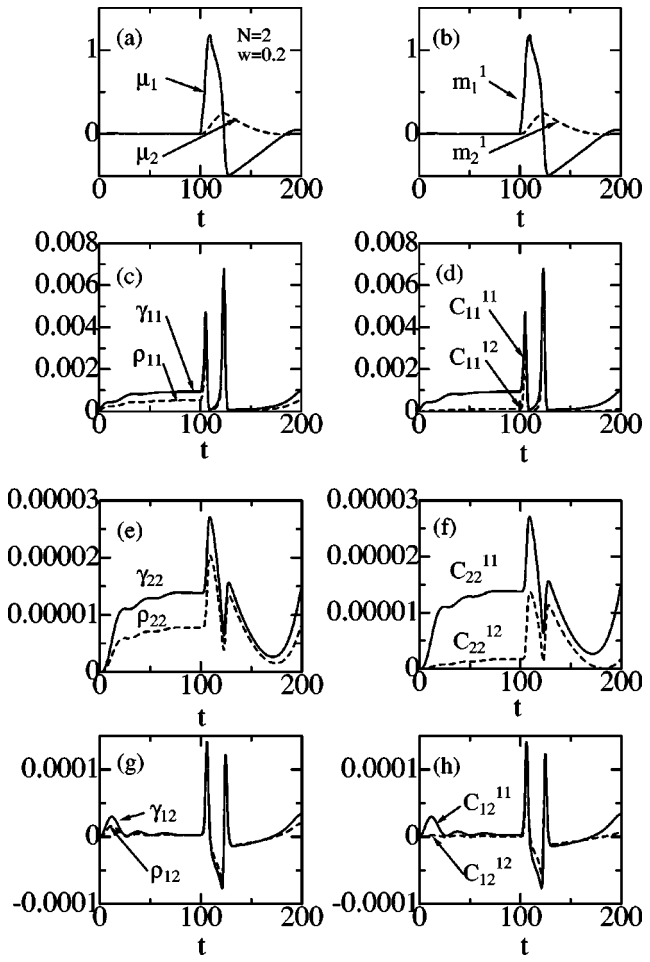

FIG. 11. A numerical comparison between DMA and moment methods for $N=2$ with $A=0.10$, $\beta=0.01$, and $w=0.2$: (a) μ_1 and μ_2, (b) m_1^i and m_2^i, (c) $\gamma_{1,1}$ and $\rho_{1,1}$, (d) $C_{1,1}^{i,j}$, (e) $\gamma_{2,2}$ and $\rho_{1,1}$, (f) $C_{2,2}^{i,j}$, (g) $\gamma_{1,2}$ and $\rho_{1,2}$, and (h) $C_{1,2}^{i,j}$ $(i,j=1,2)$. Results of DMA agree with those of the moment method (see text).

$$\frac{d\gamma_{1,1}}{dt}=2[(f_1+3f_3\gamma_{1,1})\gamma_{1,1}-c\gamma_{1,2}]+2w\left(\rho_{1,1}-\frac{\gamma_{1,1}}{2}\right)U_1+\beta^2, \tag{B29}$$

$$\frac{d\gamma_{2,2}}{dt}=2(b\gamma_{1,2}-d\gamma_{2,2}), \tag{B30}$$

$$\frac{d\gamma_{1,2}}{dt}=b\gamma_{1,1}+(f_1+3f_3\gamma_{1,1}-d)\gamma_{1,2}-c\gamma_{2,2}+w\left(\rho_{1,2}-\frac{\gamma_{1,2}}{2}\right)U_1, \tag{B31}$$

$$\frac{d\rho_{1,1}}{dt}=2[(f_1+3f_3\gamma_{1,1})\rho_{1,1}-c\rho_{1,2}]+w\rho_{1,1}U_1+\frac{\beta^2}{2}, \tag{B32}$$

$$\frac{d\rho_{2,2}}{dt}=2(b\rho_{1,2}-d\rho_{2,2}), \tag{B33}$$

$$\frac{d\rho_{1,2}}{dt}=b\rho_{1,1}+(f_1+3f_3\gamma_{1,1}-d)\rho_{1,2}-c\rho_{2,2}+\left(\frac{1}{2}\right)w\rho_{1,2}U_1, \tag{B34}$$

where $U_0=g_0+g_2\gamma_{1,1}$ and $U_1=g_1+3g_3\gamma_{1,1}$.

Figures 11(a)–11(h) show the numerical comparison between DMA and moment methods for a typical set of model parameters of $\beta=0.01$, $w=0.2$, and $N=2$ with an external input given by Eq. (3) for $A=0.1$, $t_{in}=100$, and $T_w=10$. Left panels [Figs. 11(a), 11(c), 11(e), and 11(g)] express results in DMA and right panels [Figs. 11(b), 11(d), 11(f), and 11(h)] those in the moment method. We note that our model satisfies the condition given by Eqs. (49) and (50), for which DMA and the moment method yield the same result for the averaged quantities given by $\mu_\kappa=\overline{\mu_\kappa}\equiv(1/2)(m_\kappa^1+m_\kappa^2)$, $\gamma_{\kappa,\lambda}=\overline{\gamma_{\kappa,\lambda}}\equiv(1/2)(C_{\kappa,\lambda}^{1,1}+C_{\kappa,\lambda}^{1,1})$, and $\rho_{\kappa,\lambda}=\overline{\rho_{\kappa,\lambda}}\equiv(1/4)(C_{\kappa,\lambda}^{1,1}+C_{\kappa,\lambda}^{1,2}+C_{\kappa,\lambda}^{2,1}+C_{\kappa,\lambda}^{2,2})$ for $N=2$. Actually, Figs. 11(a) and 11(b) show that $\mu_1=m_1^1=m_1^2$ and $\mu_2=m_2^1=m_2^2$. Figure 11(c) expresses $\gamma_{1,1}$ and $\rho_{1,1}$, which consist of intrasite $(C_{1,1}^{1,1}=C_{1,1}^{2,2})$ and intersite components $(C_{1,1}^{1,2}=C_{1,1}^{2,1})$ shown in Figs. 11(d). For an adopted value of $w=0.2$, the intersite (1,1) component of $C_{1,1}^{1,2}=C_{1,1}^{2,1}$, which vanishes for $w=0$, has an appreciable magnitude comparable to $C_{1,1}^{1,1}=C_{1,1}^{2,2}$, while an input is applied at $100\leqslant t\leqslant 110$. This is true also for intersite (2,2) components $(C_{2,2}^{1,2}=C_{2,2}^{2,1})$ and (1,2) components $(C_{1,2}^{1,2}=C_{1,2}^{2,1})$, which are shown in Figs. 11(e)–11(h). Calculated results of DMA and moment methods are in good agreement with those of simulations (not shown).

APPENDIX C: DERIVATION OF EQ. (59)

The distribution $P(x_i)$ in Eq. (59) is formally given by

$$P(x_i)=\int\cdots\int\Pi_{j(\neq i)}dx_j\Pi_j dy_j \times p(x_1,\ldots,x_N,y_1,\ldots,y_N), \tag{C1}$$

with the Gaussian distribution function (pdf) of $p(x_1,\ldots,x_N,y_1,\ldots,y_N)$ for the $2N$-dimensionl vector $\mathbf{z}=(x_1,\ldots,x_N,y_1,\ldots,y_N)^t$, given by

$$p(x_1,\ldots,x_N,y_1,\ldots,y_N)=\frac{1}{(2\pi)^N\sqrt{|\mathbf{V}|}}\exp\left[-\frac{1}{2}(\mathbf{z}-\boldsymbol{\mu})^t\mathbf{V}^{-1}(\mathbf{z}-\boldsymbol{\mu})\right], \tag{C2}$$

where $\boldsymbol{\mu}$ and $\mathbf{V}$ express the mean vector and the variance-covariance matrix, respectively,

In the case of a single FN neuron $(N=1)$, pdf is given by

$$p(x_1,y_1)=p_1(x_1,y_1)=\frac{1}{(2\pi)\sqrt{|\mathbf{V}|}}\exp\left[-\frac{1}{2}(\mathbf{z}-\boldsymbol{\mu})^t\mathbf{V}^{-1}(\mathbf{z}-\boldsymbol{\mu})\right], \tag{C3}$$

with

$$\mathbf{z}=(x_1,y_1)^t, \tag{C4}$$

$$\boldsymbol{\mu}=(\mu_1,\mu_2)^t, \tag{C5}$$

$$\mathbf{V}=\begin{pmatrix}\gamma_{1,1} & \gamma_{1,2}\\ \gamma_{1,2} & \gamma_{2,2}\end{pmatrix}. \tag{C6}$$

Substituting Eqs. (C3)–(C6) into Eq. (C1), we get

$$P(x_1)=\int dy_1 p(x_1,y_1)=\frac{1}{\sqrt{\gamma_{1,1}}}\phi\left(\frac{x_1-\mu_1}{\sqrt{\gamma_{1,1}}}\right), \tag{C7}$$

where $\phi(x)$ denotes the normal distribution function,

$$\phi(x)=\frac{1}{\sqrt{2\pi}}\exp\left(-\frac{x^2}{2}\right). \tag{C8}$$

In the case of arbitrary N under consideration, the calculation of $P(x_i)$ may be performed within DMA as follows. As mentioned in Sec. II C, our DMA theory assumes the configuration in which a *single* neuron is embedded in an effective medium characterized by μ_κ, $\gamma_{\kappa,\lambda}$, and $\rho_{\kappa,\lambda}$ [Eqs. (54)–(56)]. Thus, it is effectively the problem of a single neuron in the effective medium. Means μ_κ, variances $\gamma_{\kappa,\kappa}$, and covariances $\gamma_{\kappa,\lambda}$ of local variables are determined by Eqs. (20)–(24). Then the calculation of $P(x_i)$ for $N>1$ is the same as that for $N=1$ mentioned above, and it is given by

$$P(x_i)=\int dy_1 p(x_1,y_1)=\frac{1}{\sqrt{\gamma_{1,1}}}\phi\left(\frac{x_i-\mu_1}{\sqrt{\gamma_{1,1}}}\right). \tag{C9}$$

APPENDIX D: DERIVATION OF EQ. (69)

Equations (20), (21), and (25)–(27) form DEs for means μ_κ, variances $\rho_{\kappa,\kappa}$, and covariances $\rho_{\kappa,\lambda}$ for global variables, X and Y. Then $P(X)$ in Eq. (69) is given by

$$P(X)=\int dY p(X,Y), \tag{D1}$$

with pdf for the two-dimensional vector $\mathbf{z}=(X,Y)^t$ given by

$$p(X,Y)=\frac{1}{2\pi\sqrt{|\mathbf{V}|}}\exp\left[-\frac{1}{2}(\mathbf{z}-\boldsymbol{\mu})^t\mathbf{V}^{-1}(\mathbf{z}-\boldsymbol{\mu})\right], \tag{D2}$$

with

$$\boldsymbol{\mu}=(\mu_1,\mu_2)^t, \tag{D3}$$

$$\mathbf{V}=\begin{pmatrix}\rho_{1,1} & \rho_{1,2}\\ \rho_{1,2} & \rho_{2,2}\end{pmatrix}. \tag{D4}$$

Substituting Eqs. (D2)–(D4) in Eq. (D1), we obtain

$$P(X)=\frac{1}{\sqrt{\rho_{1,1}}}\phi\left(\frac{X-\mu_1}{\sqrt{\rho_{1,1}}}\right), \tag{D5}$$

where $\phi(x)$ denotes the normal distribution [Eq. (C8)].

Alternatively, $P(X)$ is expressed by

$$P(X)=\int\cdots\int \Pi_i dx_i \Pi_i dy_i p(x_1,\ldots,x_N,y_1,\ldots,y_N)\times\delta\left(X-\frac{1}{N}\sum_i x_i\right), \tag{D6}$$

where $p(x_1,\ldots,x_N,y_1,\ldots,y_N)$ stands for pdf for $2N$-dimensional vector [Eq. (C2)]. However, a calculation of $P(X)$ based on Eq. (D6) is difficult, except for the no coupling case ($w=0$), for which pdf is given by

$$p(x_1,\ldots,x_N,y_1,\ldots,y_N)=\Pi_i p_1(x_i,y_i), \tag{D7}$$

$p_1(x_i, y_i)$ being pdf for $N=1$ [Eq. (C3)]. Performing integrals with respect to y_i in Eq. (D6) with Eq. (D7), we get

$$P(X)=\int\cdots\int \Pi_i dx_i \Pi_i \frac{1}{\sqrt{\gamma_{1,1}}}\phi\left(\frac{x_i-\mu_1}{\sqrt{\gamma_{1,1}}}\right)\times\delta\left(X-\frac{1}{N}\sum_i x_i\right). \tag{D8}$$

By using the procedure conventionally used for proving the central-limit theorem, we obtain Eq. (D5) with $\rho_{1,1}=\gamma_{1,1}/\sqrt{N}$ (for $w=0$). We should note that a calculation of $P(X)$ based on Eq. (D1) is easier than that based on Eq. (D6) and that the former is applicable for finite couplings.

APPENDIX E: ANALYSIS OF NOISE, COUPLING, AND SIZE DEPENDENCE

1. $\delta t_{o\ell}$ and δt_{og}

Based on the calculated results of DMA theory, we have tried to obtain the analytical expression of the β, w, and N dependence of $\delta t_{o\ell}$ and δt_{og}. Figures 3(a) and 3(b) show that $\delta t_{o\ell}$ and δt_{og} are proportional to β for weak noises, for which both $\gamma_{1,1}$ and $\rho_{1,1}$ are proportional to β^2 [see Eqs. (61), (66), (70), and (73)]. From results shown in Figs. 4 and 5, we have obtained expressions given by

$$\frac{\delta t_{o\ell}(w,N)}{\delta t_{o\ell}(0,1)}\sim 1-\left(\frac{1}{2}\right)\left(1-\frac{1}{N}\right)^n(a_1 w+a_2 w^2+\cdots), \tag{E1}$$

$$\frac{\delta t_{og}(w,N)}{\delta t_{o\ell}(0,1)}\sim\frac{1}{\sqrt{N}}, \tag{E2}$$

where $n=1$, $\delta t_{o\ell}(0,1)=2.71$, $a_1=7.0$, and $a_2=-11.0$. The N dependence of $\delta t_{o\ell}$ expressed by Eq. (E1) with $n=1$ and 2 are shown by thin solid curves at the uppermost part in Fig. 4(b) with DMA result (small filled squares): these results are shifted upward by 0.433 for clarity of the figure. The result

with $n=1$ in better agreement with the DMA result than that with $n=2$. On the other hand, bold, dashed curves in Figs. 5(a) and 5(b) show the w dependence of $\delta t_{o\ell}$ for $N=100$ and 10, respectively, expressed by Eq. (E1) with $n=1$, which is in good agreement with results of DMA theory shown by filled squares. This implies from Eqs. (61), (66), (70), and (73) that the w and N dependence of $\gamma_{1,1}$ and $\rho_{1,1}$ evaluated at $t=t_o^*$, where $\mu_1(t_o^*)=\theta$, are given by

$$\frac{\gamma_{1,1}(w,N)}{\gamma_{1,1}(0,1)} \sim 1-\left(1-\frac{1}{N}\right)(a_1 w + a_2 w^2 + \cdots), \quad \text{(E3)}$$

$$\frac{\rho_{1,1}(w,N)}{\gamma_{1,1}(0,1)} \sim \frac{1}{N}. \quad \text{(E4)}$$

Note that $\delta t_{o\ell}(0,1)$ and $\gamma_{1,1}(0,1)$ are proportional to β and β^2, respectively.

2. S_{max}

In order to discuss the expression of β, w, and N dependent S_{max}, we have analyzed results of S_{max} shown in Fig. 7 by

$$S_{max} = c_1 w + c_2 w^2 + \cdots \quad \text{(E5)}$$

to guess how expansion coefficients of c_1 and c_2 depend on N. After several trials, we have concluded that the w and N dependence of $\gamma_{1,1}$ and $\rho_{1,1}$ evaluated at $t=t_o^{(m)}$, where $\rho_{1,1}(t)$ has the maximum value, may be given by

$$\frac{\gamma_{1,1}(w,N)}{\gamma_{1,1}(0,1)} \sim 1-\left(1-\frac{1}{N}\right)^m (b_1 w + b_2 w^2 + \cdots), \quad \text{(E6)}$$

$$\frac{\rho_{1,1}(w,N)}{\gamma_{1,1}(0,1)} \sim \frac{1}{N} \quad \text{(E7)}$$

yielding S_{max} given by [see Eq. (77)]

$$S_{max}(w,N) = \left(\frac{1}{N}\right)\left(1-\frac{1}{N}\right)^{m-1} \times \left\{ b_1 w + \left[b_2 + \left(1-\frac{1}{N}\right)^2 b_1^2 \right] w^2 \right\}, \quad \text{(E8)}$$

where $m=2$, $b_1=22$, and $b_2=-290$. Bold, dashed curves in Fig. 7 show the w dependence of S_{max} expressed by Eq. (E8) for various N values, which are in fairly good agreement with results of DMA theory shown by solid curves. We should point out that a factor of $(1-1/N)$ in Eqs. (E1), (E3), (E6), and (E8) appears because the coupling w does not work in a single-neuron case ($N=1$) and that at least the second power ($m=2$) is necessary in Eq. (E6) for S_{max} to vanish in the $N=1$ limit. A functional form of Eq. (E3) may be different from that of Eq. (E6) because the former is evaluated at t_o^*, while the latter at $t_o^{(m)}$. Our DMA calculation shows that when β is increased for a fixed (finite) w value, S_{max} is gradually decreased, although Eq. (E8) has no β dependence. This is due to contributions of $O(\beta^4)$ to $\gamma_{1,1}$ and $\rho_{1,1}$, which have not been included in the above discussion.

[1] F. Rieke, D. Warland, R. Steveninck, and W. Bialek, *Exploring the Neural Code* (MIT Press, Cambridge, MA, 1996).
[2] R.C. deCharms Proc. Natl. Acad. Sci. U.S.A. **95**, 15 166 (1998).
[3] J.J. Eggermont, Neurosci. Biobehav Rev. **22**, 355 (1998).
[4] W.M. Ursey and R.C. Reid, Annu. Rev. Physiol. **61**, 435 (1999).
[5] R.C. deCharms and A. Zador, Annu. Rev. Neurosci. **23**, 613 (2000).
[6] A. Pouget, P. Dayan, and R. Zemel, Nat. Neurosci. **1**, 125 (2000).
[7] E.D. Adrian, J. Physiol. (London) **61**, 49 (1926).
[8] W.R. Softky and C. Koch, J. Neurosci. **13**, 334 (1993).
[9] P. König, A.K. Engel, and W. Singer, Trends Neurosci. **19**, 130 (1996).
[10] C.F. Stevens and A.M. Zador, Nat. Neurosci. **1**, 210 (1998).
[11] C.E. Carr, W. Heiligenberg, and G.J. Rose, J. Neurosci. **6**, 107 (1986).
[12] R. Eckhorn, R. Bauer, W. Jordan, M. Brosch, W. Kruse, M. Munk, and H.J. Reitboeck, Biol. Cybern. **60**, 121 (1988).
[13] C.M. Gray and W. Singer, Proc. Natl. Acad. Sci. U.S.A. **86**, 1698 (1989).
[14] E.T. Rolls and M.J. Tovee, Proc. R. Soc. London, Ser. B **257**, 9 (1994).
[15] S. Thorpe, D. Fize, and C. Marlot, Nature (London) **381**, 520 (1996).
[16] L. Abbott and T. J. Sejnowski, *Neural Codes and Distributed Representations* (MIT Press, Cambridge, MA, 1998).
[17] J.J. Hopfield, Nature (London) **376**, 33 (1995).
[18] D. Horn and S. Levanda, Neural Comput. **10**, 1705 (1998).
[19] R. van Rullen and S.J. Thorpe, Neural Comput. **13**, 1255 (2001).
[20] C.M. Gray and W. Singer, Proc. Natl. Acad. Sci. U.S.A. **86**, 1698 (1989).
[21] N. Hatsopoulas, C.L. Ojakangas, L. Paninski, and J.P. Donohue, Proc. Natl. Acad. Sci. U.S.A. **95**, 15 706 (1998).
[22] R.C. deCharmes and M.M. Merzenich, Nature (London) **381**, 610 (1996).
[23] Z.F. Mainen and T.J. Sejnowski, Science **268**, 1503 (1995).
[24] L. Gammaitoni, P. Hänggi, P. Jung, and F. Marchesoni, Rev. Mod. Phys. **70**, 223 (1998).
[25] V.S. Anishchenko, A.B. Neiman, F. Moss, and L. Schimansky-Geier Usp. Fiz. Nauk. **169**, 7 (1999) [Phys. Usp. **42**, 7 (1999)].
[26] J. P. Segund, J. F. Vibert, K. Pakdaman, M. Stiber, and O. Diez-Martinez, in *Origins; Brain and Self Organization*, edited by K. Pribram (Lawrence Erlbaum, Mahwah, NJ, 1994), pp. 299–331.
[27] S. Tanabe, S. Sato, and K. Pakdaman, Phys. Rev. E **60**, 7235 (1999).
[28] S. Tanabe and K. Pakdaman, Biol. Cybern. **85**, 269 (2001).
[29] S. Tanabe and K. Pakdaman, Phys. Rev. E **64**, 041904 (2001).
[30] X. Pei, L. Wilkens, and F. Moss, Phys. Rev. Lett. **77**, 4679 (1996).

[31] J.J. Collins, C.C. Chow, and T.T. Imhoff, Nature (London) **376**, 236 (1995).
[32] D.R. Chialvo, A. Longtin, and J. Müller-Gerking, Phys. Rev. E **55**, 1798 (1997).
[33] T. Shimokawa, A. Rogel, K. Pakdaman, and S. Sato, Phys. Rev. E **59**, 3461 (1999).
[34] H. Hasegawa, Phys. Rev. E **66**, 021902 (2002).
[35] H. Hasegawa, e-print cond-mat/0202252.
[36] D. Hansel, G. Mato, M. Meunier, and L. Nelteur, Neural Comput. **10**, 467 (1998).
[37] Y. Kuramoto, Physica D **50**, 15 (1991).
[38] L.F. Abbott and C. van Vreeswijk, Phys. Rev. E **48**, 1483 (1993).
[39] A. Treves, Network **4**, 259 (1993).
[40] W. Gerstner, Phys. Rev. E **51**, 738 (1995).
[41] A. Omurtag, B.W. Knight, and L. Sirovich, J. Comput. Neurosci. **8**, 51 (2000).
[42] E. Haskell, D.Q. Nykamp, and D. Tranchina, Network **12**, 141 (2000).
[43] R. Rodriguez and H.C. Tuckwell, Phys. Rev. E **54**, 5585 (1996).
[44] H.C. Tuckwell and R. Rodriguez, J. Comput. Neurosci. **5**, 91 (1998).
[45] R. Rodriguez and H.C. Tuckwell, BioSystems **48**, 187 (1998).
[46] R. Rodriguez and H.C. Tuckwell, Math. Comput. Model. **31**, 175 (2000).
[47] S. Tanabe and K. Pakdaman, Phys. Rev. E **63**, 31 911 (2001).
[48] R. FitzHugh, Biophys. J. **1**, 445 (1961).
[49] J. Nagumo, S. Arimoto, and S. Yoshizawa, Proc. IRE **50**, 2061 (1962).
[50] A. Longtin, J. Stat. Phys. **70**, 309 (1993).
[51] K. Wiesenfeld, D. Pierson, E. Pantazelou, C. Dames, and F. Moss, Phys. Rev. Lett. **72**, 2125 (1994).
[52] A. Longtin and D.R. Chialvo, Phys. Rev. Lett. **81**, 4012 (1994).
[53] T. Kanamaru, T. Horita, and Y. Okabe, Phys. Rev. E **64**, 031908 (2000).
[54] N.G. Stocks and R. Mannella, Phys. Rev. E **64**, 030902 (2001).
[55] P. Weiss, J. Phys. Radium **4**, 661 (1947).
[56] P. Soven, Phys. Rev. **156**, 809 (1967); B. Velický, S. Kirkpatrick, and H. Ehrenreich, *ibid.* **175**, 747 (1968).
[57] In the case of multiple subclusters discussed in Sec. IV, the average of $\langle Q(\mathbf{z},t)\rangle$ of an arbitrary function $Q(\mathbf{z})$ is formally given in the same way as shown in Eq. (8) (but with the dimension of $2\sum_m N_m$). When the variable $\mathbf{z}=(0,\ldots,0,\mathbf{z}_m,0,\ldots,0)^t$ includes only the component $\mathbf{z}_m$ relevant to the subcluster m, the average is given by $\langle Q(\mathbf{z},t)\rangle = \int\cdots\int d\mathbf{z}_m Q(\mathbf{z},t)p(\mathbf{z}_m)$, where $p(\mathbf{z}_m)$ denotes pdf expressed by the $n=2N_m$-dimensional variable $\mathbf{z}_m=(z_1,\ldots,z_n)^t$. Then the problem reduces to the single-cluster case discussed in Sec. II.
[58] H.R. Wilson and J.D. Cowan, Kybernetik **13**, 55 (1973).
[59] M. Abeles, H. Bergman, E. Margalit, and E. Vaadia, J. Neurophysiol. **70**, 1629 (1993).
[60] In the moment method, the number of DEs is $N_{eq}=NK+(1/2)NK(NK+1)=(1/2)NK(NK+3)$, which is 14, 860, 80 600, and 8 006 000 for $N=1$, 10, 100, and 1000, respectively, with $K=4$.
[61] H. Hasegawa, e-print cond-mat/0302502.
[62] M. Diesmann, M. Gewaltig, and A. Aertsen, Nature (London) **402**, 529 (1999).
[63] B. Hu and C. Zhou, Phys. Rev. E **61**, R1001 (2000); G. De Vries and A. Sherman, Bull. Math. Biol. **63**, 371 (2001); C.D. Boschi, E. Louis, and G. Ortega, Phys. Rev. E **65**, 012901 (2001).